

Fermion-fermion interaction driven instability and criticality of quadratic band crossing systems with the breaking of time-reversal symmetry

Ya-Hui Zhai and Jing Wang*

Department of Physics, Tianjin University, Tianjin 300072, People's Republic of China

(Dated: December 7, 2020)

Roles of fermion-fermion interactions are carefully studied in governing the low-energy fates of a two-dimensional spin-1/2 fermionic system on the kagomé lattice, which features a quadratic band crossing point touched parabolically by up and down energy bands. In the framework of a renormalization group, we establish the coupled energy-dependent flows of fermionic interaction parameters by treating all kinds of fermionic interactions on the same footing and unbiasedly taking into account their one-loop corrections. Through an analysis of these evolutions that carry the hierarchical information of physics, a number of interesting behaviors are progressively decoded and addressed manifestly in the low-energy regime. At first, we find that various sorts of fermion-fermion interactions furiously compete and affect each other. With the decrease of energy scale, they are inevitably attracted by certain fixed point in the parameter space which clusters into three qualitatively distinct regions relying heavily upon structure parameters of materials. In addition, the leading instability accompanied by some symmetry breaking is attentively investigated in the proximity of different sorts of fixed points. Computing and comparing susceptibilities of twelve potential candidates indicates that charge density wave always dominates over others. Incidentally, there exists several options for subleading ones including the x -current, bond density, and chiral plus s -wave superconductors. At last, we examine how physical observables behave nearby the dominant instability. Due to the strong fluctuations neighboring this instability linked to charge density wave, density of states and specific heat as well compressibility of quasiparticles are significantly suppressed in the lowest-energy limit.

PACS numbers: 71.10.-w, 71.70.Gm, 71.55.Ak, 64.60.ae

I. INTRODUCTION

Past two decades have witnessed a phenomenally rapid development of semimetal materials^{1–12} that feature well-known discrete Dirac points accompanied by gapless quasi-particle excitations and linear energy dispersions along two or three directions^{1–9,12–21}. The list consists of Dirac semimetals^{22–27} and Weyl semimetals^{2,28–35} as well as their semi-Dirac cousins^{36–41}. In recent years, interest has gradually shifted from linear-dispersion toward quadratic-dispersion fermi materials with up and down bands parabolically touching at certain quadratic band crossing point (QBCP) for both two^{42–56} and three dimensions^{18,57–72}. Compared to their Dirac/Weyl counterparts with the vanishment of density of state (DOS) at Dirac points, two-dimensional (2D) QBCP materials attract more attention and become one of the most active subjects^{42–44,47–49,54,55}. The main reason is ascribed to the finite density of states at the Fermi surface together with its unique gapless quasiparticles (QPs) from discrete QBCPs developed by the crossings of up and down parabolical bands, leading to the possibility of weak coupling interaction-driven instability^{44,48,51,52}. These 2D QBCP materials are suggested to be realized on some collinear spin density wave state⁷³, Lieb lattice⁷⁴, checkerboard^{43,48} and kagomé lattices^{44,55,75} with distinct kinds of symmetries under point group consideration^{44,47,48}.

What is more, 2D QBCP systems are allowed to either host the time-reversal symmetry (TRS) or present

the TRS breaking depending upon concrete lattices. On one side, the free Hamiltonian of 2D QBCP semimetals rooted in the checkerboard lattice is protected by TRS^{44,47,48}. With respect to these materials, unconventional band structures and gapless QPs in tandem with weak couplings yield to many fascinating behaviors in the low-energy regime^{44–46,48,50,51,76,77}. In particular, quantum anomalous Hall (QAH) and quantum spin Hall (QSH) can be generated by fermion-fermion repulsions on the checkerboard lattice^{44,48} or two-valley bilayer graphene with QBCPs^{45,46}, as well as their low-energy stabilities under the impacts of impurity scatterings are also examined^{51,52}. On the other side, the 2D noninteracting QBCP model that originates from the kagomé lattice might be TRS breaking⁷⁵. Although this case is equipped with the similar QBCP and quadratic dispersion, its low-energy physics has hitherto been insufficiently explored. Given the basic structure of free Hamiltonian is quite far away from its checkerboard counterpart, a number of tempting questions concerning the kagomé-lattice version naturally arise: whether and how the low-energy physical properties are influenced by fermion-fermion interaction? Whether they can activate the instabilities? Which states are the suitable candidates and what are the critical behaviors in the vicinity of potential instabilities? It would be instructive to deepen our understanding of the 2D QBCP materials once these inquiries are properly answered.

Inspired by these, we within this work put our focus on a 2D QBCP spin-1/2 fermionic system on the kagomé lattice and investigate its low-energy fate in the presence

of 16 types of marginal fermion-fermion interactions. In order to treat all these physical ingredients on an equal footing, we employ the momentum-shell renormalization-group (RG) approach^{78–80}, which is a powerful tool to refine and characterize the hierarchical physics in the concomitant presence of various types of interactions. Practicing the standard procedures of RG framework gives rise to the one-loop energy-dependent evolutions of all fermion-fermion interaction parameters. With the help of these RG flows that encode the energy-dependent physics, several intriguing critical behaviors are extracted in the low-energy regime.

At first, we, with the help of the numerical analysis of RG equations, are aware that fermionic interactions are of close relevance to each other and evolve towards strong couplings due to their intimate interplay at certain energy scale. Considering the degenerate trajectories of several kinds of interactions, we only need to put our focus on six nontrivial fermionic couplings that flow independently. To overcome the strong couplings and make our study perturbative, we follow the strategy put forward in Refs.^{45,48}. Concretely, we select a non-sign changed coupling to rescale the six nontrivial parameters and are left with relative evolutions together with the corresponding relatively fixed points living in the parameter space which are conventionally in charge of singular properties.

Next, we figure out that the concrete values of relatively fixed points are insusceptible to initial conditions of fermion-fermion interactions but instead primarily determined by two structure parameters d_1 and d_3 in the Hamiltonian. Adjusting the ratio between these two quantities yields to three qualitative different regions at which the relatively fixed points exhibit diverse traits. Since the relatively fixed point is related to some instability that is always accompanied by certain symmetry breaking and thus some phase transition^{47,48,51,81–88}, it is therefore of intense interest to identify which is the leading instability for the relatively fixed point residing in different regions. To this end, we introduce the source terms of twelve kinds of potential candidates and evaluate their related susceptibilities approaching a relatively fixed point^{47,48,51}. Carrying out both the theoretical and numerical analysis indicates that the charge density wave always takes a leading role in the whole region. In addition, four subleading ones involving the x -current, bond density, and chiral or s -wave superconductors largely hinge upon the relatively fixed points.

Moreover, the critical properties of physical implications are briefly studied around the leading instability. We notice that ferocious fluctuations induced by the development of charge density wave are generally detrimental for density of states and specific heat as well compressibility of quasiparticles. It is worth pointing out that these quantities are all substantially reduced and even drive to zero while the dominant order parameter triggered by the divergent instability is large enough^{82,89–94}.

The rest of paper is organized as follows. In Sec II A,

we present the microscopic model for 2D QBCP spin-1/2 electronic system on the kagomé lattice and construct our effective action consisting of both free terms and all marginal fermion-fermion interactions. Starting from this effective theory, we within Sec. II B carry out one-loop momentum-shell RG analysis and derive the coupled RG equations of all fermionic interaction parameters. By virtue of numerical analysis of RG evolutions, Sec. III is followed to seek and classify the underlying fixed points in the low-energy regime. In addition, we bring out the source terms in Sec. IV and pinpoint the dominant and subleading instabilities nearby distinct types of relatively fixed points. Furthermore, critical behaviors of physical quantities activated by ferocious fluctuations are concisely investigated in Sec. V. Finally, Sec. VI briefly summarizes our central points.

II. EFFECTIVE THEORY AND RG ANALYSIS

At the outset, we are going to present the microscopic model and build the effective theory in the low-energy regime as well as establish the coupled energy-dependent flow equations of all marginal fermion-fermion couplings by carrying out the standard momentum-shell RG framework^{78–80}.

A. Effective theory

We hereafter concentrate on the 2D spin-1/2 electronic system stemming from the kagomé lattice that is characterized by a QBCP at which up and down energy bands parabolically meet^{44,75}. Accordingly, its non-interacting Hamiltonian that captures the low-energy fermionic excitations nearby the QBCP can be written as^{44,75},

$$H_0 = \sum_{|\mathbf{k}| < \Lambda} \Psi_{\mathbf{k}}^\dagger \mathcal{H}_0(\mathbf{k}) \Psi_{\mathbf{k}}, \quad (1)$$

where Λ serves as the momentum cutoff and the Hamiltonian density is casted as⁷⁵

$$\mathcal{H}_0(\mathbf{k}) = d_3 \mathbf{k}^2 \Sigma_{03} + d_1 (k_x^2 - k_y^2) \Sigma_{01} + d_2 k_x k_y \Sigma_{02}, \quad (2)$$

with d_1 , d_2 , and d_3 being microscopic structure parameters of continuum Hamiltonian. Hereby, $\Psi^\dagger = (c_{1\uparrow}^\dagger, c_{1\downarrow}^\dagger, c_{2\uparrow}^\dagger, c_{2\downarrow}^\dagger)$ is designated as a four-component spinor to specify the low-energy quasiparticles coming from two energy bands and unequal spins^{44,75}. In addition, the 4×4 matrix $\Sigma_{\mu\nu} \equiv \tau_\mu \otimes \sigma_\nu$, where τ_μ and σ_ν with $\mu, \nu = 0, 1, 2, 3$ represent Pauli matrices $\tau_{1,2,3}$, $\sigma_{1,2,3}$ and identity matrix τ_0, σ_0 , is employed to act on both the spin space and lattice space. Without loss of generality, we take $d_2 \equiv 2d_1$ to simplify our analysis⁷⁵ (the basic results are robust against certain simplification). In this

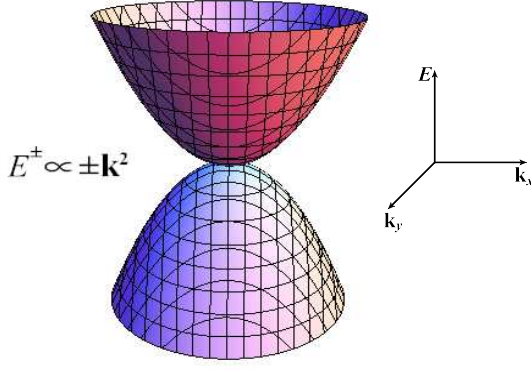


FIG. 1: (Color online) Schematic illustration of the 2D QBCP band structure with a quadratic band crossing point parabolically touched by the up and down energy bands.

respect, the parabolical energy eigenvalues are directly obtained after diagonalizing the free Hamiltonian (1)

$$E^\pm(\mathbf{k}) = \pm \mathbf{k}^2 \sqrt{d_1^2 + d_3^2}, \quad (3)$$

with \pm specifying the upward and downward bands that quadratically touch at $\mathbf{k} = 0$ as schematically shown in Fig. 1.

As aforementioned, it has attracted much interest to investigate the impacts of fermion-fermion interactions

on the low-energy fates of 2D QBCP systems locating at checkerboard lattices^{44,45,48,51,52,95,96}. However, compared to its checkerboard counterpart^{43,48}, we need to bear in mind that the 2D QBCP model (2) with the TRS breaking is still inadequately explored despite of holding the particle-hole symmetry and sixfold rotational symmetry^{44,75}. Due to the qualitative difference of microscopic structures between kagomé and checkerboard lattices, we therefore within this work endeavor to verify how the fermion-fermion interactions impact the low-energy properties of 2D kagomé-version QBCP systems.

To be concrete, we herein take into account all potential marginal short-range four-fermion interactions on an equal footing^{44,48,51,75}

$$S_{\text{int}} = \sum_{\mu, \nu=0}^3 \lambda_{\mu\nu} \prod_{i=1}^3 \int \frac{d\omega_i d^2\mathbf{k}_i}{(2\pi)^3} \Psi^\dagger(\omega_1, \mathbf{k}_1) \Sigma_{\mu\nu} \Psi(\omega_2, \mathbf{k}_2) \times \Psi^\dagger(\omega_3, \mathbf{k}_3) \Sigma_{\mu\nu} \Psi(\omega_1 + \omega_2 - \omega_3, \mathbf{k}_1 + \mathbf{k}_2 - \mathbf{k}_3), \quad (4)$$

where $\lambda_{\mu\nu}$ with $\mu, \nu = 0, 1, 2, 3$ are utilized to measure the coupling strengths of different types of fermion-fermion interactions that are distinguished by vertex matrixes $\Sigma_{\mu\nu}$ acting on both lattice and spin spaces.

Consequently, we are left with the effective action in the momentum space after combining the free Hamiltonian (1) and fermion-fermion interactions (4) as follows^{44,48,51}

$$S_{\text{eff}} = \int_{-\infty}^{\infty} \frac{d\omega}{2\pi} \int^{\Lambda} \frac{d^2\mathbf{k}}{(2\pi)^2} \Psi^\dagger(\omega, \mathbf{k}) [-i\omega \Sigma_{00} + d_3 \mathbf{k}^2 \Sigma_{03} + d_1(k_x^2 - k_y^2) \Sigma_{01} + d_2 k_x k_y \Sigma_{02}] \Psi(\omega, \mathbf{k}) + \sum_{\mu, \nu=0}^3 \lambda_{\mu\nu} \int_{-\infty}^{\infty} \frac{d\omega_1 d\omega_2 d\omega_3}{(2\pi)^3} \times \int^{\Lambda} \frac{d^2\mathbf{k}_1 d^2\mathbf{k}_2 d^2\mathbf{k}_3}{(2\pi)^6} \Psi^\dagger(\omega_1, \mathbf{k}_1) \Sigma_{\mu\nu} \Psi(\omega_2, \mathbf{k}_2) \Psi^\dagger(\omega_3, \mathbf{k}_3) \Sigma_{\mu\nu} \Psi(\omega_1 + \omega_2 - \omega_3, \mathbf{k}_1 + \mathbf{k}_2 - \mathbf{k}_3). \quad (5)$$

On the basis of quantum field theory, its noninteracting part directly gives rise to the free fermionic propagator⁷⁸

$$G_0(i\omega, \mathbf{k}) = \frac{1}{-i\omega + d_3 \mathbf{k}^2 \Sigma_{03} + d_1(k_x^2 - k_y^2) \Sigma_{01} + d_2 k_x k_y \Sigma_{02}}, \quad (6)$$

which plays a crucial role in constructing the RG equations.

We hereafter adopt the S_{eff} as our starting point and utilize the RG approach to inspect the low-energy behaviors of 2D spin-1/2 QBCP electric systems sitting on the kagomé lattice in the presence of these marginal fermion-fermion interactions.

B. RG analysis

We within this subsection implement the one-loop momentum-shell RG analysis⁷⁸⁻⁸⁰ to construct the entangled energy-dependent evolutions of all interaction parameters appearing in Eq. (5) that are of close relevance to the low-energy properties.

Prior to deriving the one-loop RG equations, we are forced to determine the rescaling transformations of fields, momentum and energy⁷⁸. To this end, we can select the non-interacting parts of effective action (5) as an original fixed point at which they are invariant during RG processes. As a result, we obtain the following RG rescaling transformations^{48,95,97,98}

$$k_x \longrightarrow k'_x e^{-l}, \quad (7)$$

$$k_y \longrightarrow k'_y e^{-l}, \quad (8)$$

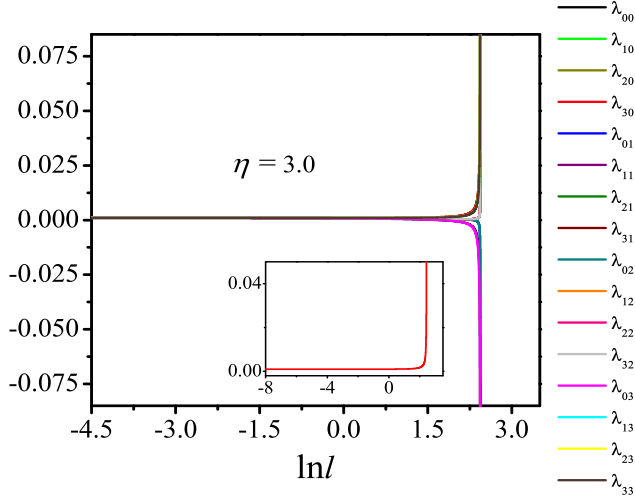


FIG. 2: (Color online) Evolutions of fermion-fermion couplings $\lambda_{\mu\nu}$ at the ratio of structure parameters $\eta = 3.0$ (the basic results are insensitive to concrete value of η). Inset: the flow of λ_{30} without sign change under the influence of fermion-fermion interactions.

$$\omega \longrightarrow \omega' e^{-2l}, \quad (9)$$

$$\Psi(i\omega, \mathbf{k}) \longrightarrow \Psi'(i\omega', \mathbf{k}') e^{3l}. \quad (10)$$

In order to grasp the contributions from fermion-fermion interactions, we have to go beyond this original fixed point and take into account all one-loop corrections. In the spirit of momentum-shell RG theory⁷⁸, the “fast modes” of fermionic fields within the momentum shell $b\Lambda < k < \Lambda$ are integrated out at first, where Λ characterizes the energy scale and variable parameter b is designated as $b = e^{-l} < 1$ with $l > 0$ being a running energy scale. Next, we insert the corrections within the momentum shell into the “slow modes” to yield the new “slow modes” and then rescale these “slow modes” to new “fast modes”^{47,48,51,81,95,97–103}. In principle, it is convenient to measure the momenta and energy with cutoff Λ_0 which is related to the lattice constant (i.e., $k \rightarrow k/\Lambda_0$ and $\omega \rightarrow \omega/\Lambda_0$) to simplify our calculations and write the results more compactly^{48,95,97,98,100,104}. To be specific, we unbiasedly take into account all one-loop Feynman diagrams depicted in Fig. 11 to capture the one-loop information of “fast modes”. After paralleling the well-trodden procedures and performing long but straightforward algebra^{48,51,95,95,96}, we obtain all one-loop corrections and present them in Appendix A for details.

Combining RG rescalings (7)-(10) and one-loop corrections (A1)-(A16), we are capable of deriving the coupled energy-dependent RG flows of interaction parameters by carrying out the standard RG analysis^{48,95,97,98} and are left with a set of sixteen coupled evolutions, namely

$$\frac{d\lambda_{\mu\nu}}{dl} = \mathcal{F}_{\mu\nu}(\lambda_{\mu\nu}, d_1, d_3), \quad (11)$$

with $\mu, \nu = 0, 1, 2, 3$ denoting all sixteen types of fermion-fermion couplings. The detailed RG equations with their

related coefficients $\mathcal{F}_{\mu\nu}(\lambda_{\mu\nu}, d_1, d_3)$ are manifestly provided in Appendix B. In the spirit of RG framework, these coupled RG equations encoding the intimate interplay of all types of fermionic interactions are of particular significance to govern the low-energy fates of 2D QBCP electronic systems. These will be attentively studied in the looming sections.

III. RELATIVE FIXED POINTS

With the coupled RG flow equations in hand, we are able to seek the underlying fixed points with lowering the energy scales, which are always assumed to dictate the critical behaviors.

A. Evolutions of interaction parameters

We start out by investigating the energy-dependent flows of four-fermion couplings, which are determined by RG equations and assumed to overarch the low-energy properties^{47,48,51,81,95,97–103}. Before proceeding, it is necessary to address several comments on the initial condition. On one hand, we, without loss of generality, treat all sixteen types of fermion-fermion interactions unbiasedly and assign them an equal beginning value. On the other hand, the RG flows also rely upon two structural parameters d_1 and d_3 . It is of particular importance to highlight that the flows are insensitive to their concrete values but instead the ratio between them. To facilitate our analysis, we hereafter designate $\eta \equiv d_3/d_1$ to capture the basic influence of these two parameters.

To proceed, taking a concrete value $\eta = 3.0$ plus a representative starting value for $\lambda_{\mu\nu}$ and performing numerical analysis of Eq. (11), we are left with the results shown in Fig. 2. Reading off this figure, we notice that fermion-fermion interactions are strongly energy-dependent and driven to be divergent at some critical energy scale denoted by l_c in the low-energy regime, which always is an unambiguous signature for emergence of phase transitions^{47,48,51,81–88}. In addition, we figure out that not all of these 16 distinct types of fermion-fermion couplings can evolve independently. It can be clearly seen from Fig. 2 that several trajectories of interaction parameters are coincident with others during the process of lowering the energy scales. To be concrete, λ_{01} is degenerate with λ_{02} and λ_{13} is coincident to λ_{23} plus λ_{33} , respectively. In particular, the tendencies of parameters λ_{10} , λ_{20} , and λ_{30} are exactly overlapped. Analogously, λ_{11} , λ_{21} , λ_{31} , λ_{12} , λ_{22} , and λ_{32} share the same evolution. As a result, all of these 16 kinds of interaction parameters cluster into six groups. In other words, there only exists six independent flows. For convenience, we from now on employ these six parameters λ_{00} , λ_{20} , λ_{01} , λ_{21} , λ_{03} , and λ_{13} to characterize all types of fermion-fermion interactions, where λ_{01} ,

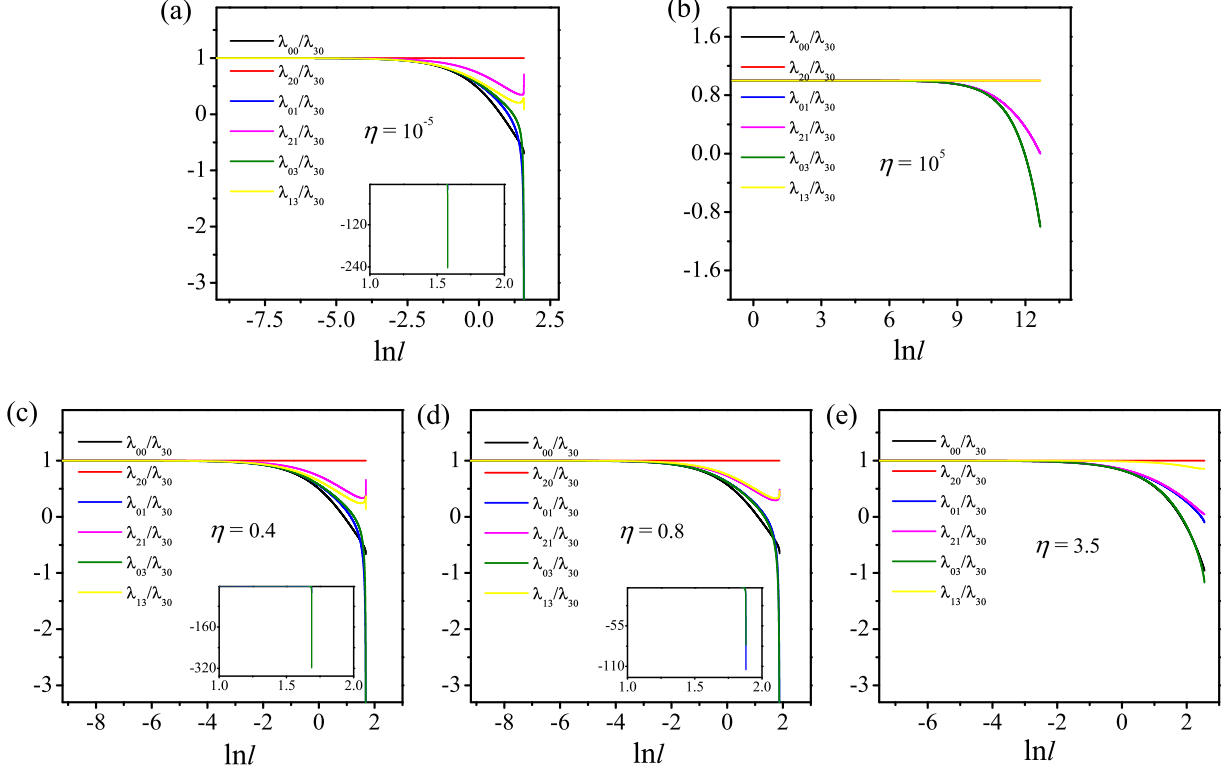


FIG. 3: (Color online) Evolutions of fermion-fermion interaction parameters $\lambda_{\mu\nu}/\lambda_{30}$ approaching: (a) Type-I-RFP at $\eta = 10^{-5}$; (b) Type-III-RFP at $\eta = 10^5$; and (c)-(e) Type-II-RFP at $\eta = 0.4$, $\eta = 0.8$, and $\eta = 3.5$, respectively.

λ_{20} , λ_{21} , and λ_{13} are chosen as four representative parameters to denote their degenerate counterparts.

B. Three η -dependent distinct regions

In light of the divergence of fermion-fermion couplings in the low-energy regime, we are conventionally suggested to rescale all parameters with a non-sign changed parameter^{45,48,51}. Based on the relative interaction parameters, one henceforth can safely work within the perturbative RG framework before the divergence^{45,48,51,81–88}.

As explicitly illustrated by inset of Fig. 2, the parameter λ_{30} flows monotonously and thus does not change sign during the entire RG flow. It is therefore convenient to measure all interaction parameters with λ_{30} . Accordingly, we from now on shift our attention to the low-energy behaviors of these relative parameters, i.e., $\lambda_{00}/\lambda_{30}$, $\lambda_{20}/\lambda_{30}$, $\lambda_{01}/\lambda_{30}$, $\lambda_{21}/\lambda_{30}$, $\lambda_{03}/\lambda_{30}$, and $\lambda_{13}/\lambda_{30}$. Besides their energy-dependent trajectories, we are of particular interest to determine the final fates of these parameters at the low-energy limit, namely, the potential fixed point (FP) which is expected to govern the physical properties and accompanied by critical behaviors. Given these parameters are rescaled by λ_{30} , we hereafter dub them relatively fixed points (RFPs)^{45,48,51}.

Although the the basic results are hardly susceptible

to starting values of fermion-fermion strengths, the flows of parameters and corresponding RFPs are heavily η -dependent. Fig. 3 manifestly shows the evolving tendencies of fermion-fermion interaction parameters strongly hinge upon the specific values of η . What is more, we learning from Fig. 4 notice that concrete values of RFPs are closely sensitive to η as well. On one side, as long as η is either tuned less than certain small value nominated as C_1 or adjusted exceed some critical value denoted as C_2 , the final values of parameters $\lambda_{\mu\nu}/\lambda_{30}$ (i.e., RFPs) arrive at some constants and then are considerably robust with lowering or increasing value of η . On the other side, the concrete values of RFPs spanning from C_1 to C_2 are no longer invariant but instead fairly rely upon η . For physical consideration, we infer that d_1 is dominant over d_3 at $\eta < C_1$ and thus the contribution from d_3 is negligible resulting in the stable values of RFPs and vice versa for $\eta > C_2$. On the contrary, neither d_1 nor d_3 can completely win its opponent within $C_1 < \eta < C_2$. It is thus the intimate competition between d_1 and d_3 that plays a pivotal role in pinning down RFPs. As unambiguously characterized in Fig. 4, the values of RFPs residing in this region are severely η -dependent.

To be specific, we directly notice that the absolute values of negative-divergent parameters $\lambda_{01}/\lambda_{30}$ and $\lambda_{03}/\lambda_{30}$ as well as the positive-divergent parameter $\lambda_{21}/\lambda_{30}$ present a clear downward trend with increasing

TABLE I: Specific values of fermion-fermion interactions with several representative ratios of structure parameters in the vicinity of three different RFPs. The corresponding energy-dependent evolutions of these couplings are manifestly displayed in Fig. 3.

RFPs	$\lambda_{00}/\lambda_{30}$	$\lambda_{20}/\lambda_{30}$	$\lambda_{01}/\lambda_{30}$	$\lambda_{21}/\lambda_{30}$	$\lambda_{03}/\lambda_{30}$	$\lambda_{13}/\lambda_{30}$	η
Type-I-RFP	-0.7	1	-20.3	0.7	-242.8	0.1	10^{-5}
Type-II-RFP	-0.7	1	-28.4	0.7	-318.1	0.1	0.4
	-0.7	1	-114.5	0.5	-81	0.5	0.8
	-1	1	-0.1	0.04	-1.2	0.9	3.5
Type-III-RFP	-1	1	0	0	-1	1	10^5

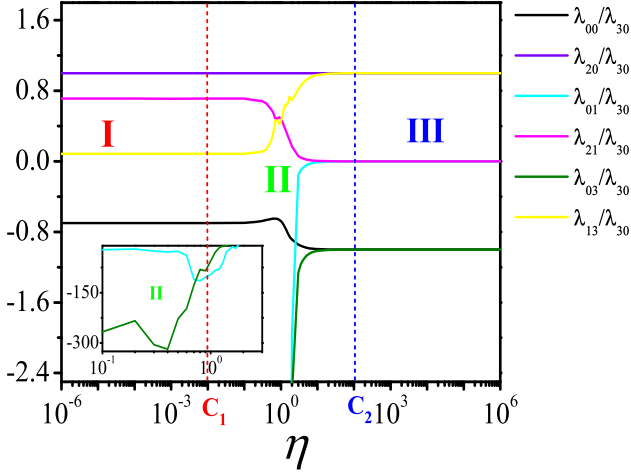


FIG. 4: (Color online) The η -dependent evolutions of fermion-fermion interaction parameters $\lambda_{\mu\nu}/\lambda_{30}$ (i.e., the concrete values of RFPs). Three distinct regions are separated by $\eta = C_1 \approx 10^{-2}$ and $\eta = C_2 \approx 10^2$, which are denominated as Type-I-Region, Type-II-Region, Type-III-Region (namely, I, II, and III), respectively.

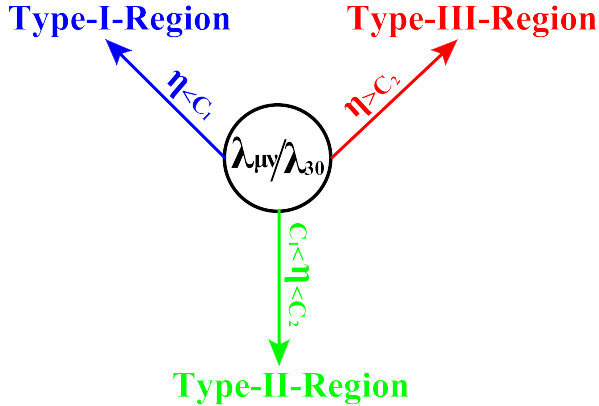


FIG. 5: (Color online) Schematic illustration of three different η -tuned regions shown in Fig. 4 with $C_1 \approx 10^{-2}$ and $C_2 \approx 10^2$. Several representative values of RFPs are presented in Table I for Type-I-Region, Type-II-Region, and Type-III-Region, respectively.

the values of η . Conversely, the increase of η is favorable to raise the absolute value of negative-divergent parameter $\lambda_{00}/\lambda_{30}$ together with positive-divergent parameters $\lambda_{13}/\lambda_{30}$. In comparison, one can readily figure out $\lambda_{20}/\lambda_{30} = 1$ is hardly susceptible to the modulation of η . In order to facilitate our studies under such circumstances, it is profitable to divide $\eta \in (0, \infty)$ into three distinct regions owing to the robustness of RFPs against the change of η . As manifestly designated in Fig. 4 and schematically illustrated in Fig. 5, they correspond to Type-I-Region ($\eta < C_1$), Type-II-Region ($C_1 < \eta < C_2$), and Type-III-Region ($\eta > C_2$), respectively.

C. Three types of relatively fixed points

Concerning the discrepancies of RFPs in these three regions, we from now on nominate the RFPs locating at Type-I-Region, Type-II-Region, and Type-III-Region as Type-I-RFP, Type-II-RFP, Type-III-RFP, respectively. In order to remedy the insufficiency of qualitative illustrations in Fig. 5, we hereby select some representative values of η with three different types of RFPs and present the specific values of the interaction parameters as collected in Table I apparently indicating their individual features. As aforementioned, the final values of interaction parameters manifested in Fig. 4 are stable in Type-I-Region and Type-III-Region under the variation of η . On the contrary, they are rather sensitive to η . Under these respects, Table I consists of only one point for both Type-I-RFP and Type-III-RFP as well as three typical points for Type-II-RFP with considering the tendency of Type-II-Region in Fig. 4.

To be concrete, Fig. 3(a) indicates that, at Type-I-RFP, the parameters $\lambda_{00}/\lambda_{30}$, $\lambda_{01}/\lambda_{30}$, and $\lambda_{03}/\lambda_{30}$ flow divergently along the negative direction. In particular, the absolute strengths of $\lambda_{03}/\lambda_{30}$ and $\lambda_{00}/\lambda_{30}$ are the strongest and weakest. However, $\lambda_{13}/\lambda_{30}$, $\lambda_{20}/\lambda_{30}$, and $\lambda_{21}/\lambda_{30}$ are sign-unchanged during the whole RG process. Compared to Type-I-RFP, $\lambda_{01}/\lambda_{30}$ and $\lambda_{21}/\lambda_{30}$ at Type-III-RFP evolve towards zero. Additionally, Fig. 3(b) shows that $\lambda_{00}/\lambda_{30}$ and $\lambda_{03}/\lambda_{30}$ are driven to be equal but opposite to $\lambda_{20}/\lambda_{30}$ and $\lambda_{13}/\lambda_{30}$ in the

TABLE II: Twelve different kinds of potential phases triggered by fermion-fermion interactions, which are associated with source-term bilinears appearing in Eq. (12)¹¹. Hereby, SC and AFM denote superconductivity and antiferromagnetism, respectively. In addition, chiral SC1 and chiral SC2 are adopted to characterize two distinct sorts of chiral superconducting states.

Order parameters	Vertex matrixes of fermionic bilinears	Potential phases
Δ_1^c	$\mathcal{M}_1^c = \tau_0 \otimes \sigma_0$	charge instability
Δ_2^c	$\mathcal{M}_2^c = \tau_0 \otimes \sigma_1$	x -current
Δ_3^c	$\mathcal{M}_3^c = \tau_0 \otimes \sigma_2$	bond density
Δ_4^c	$\mathcal{M}_4^c = \tau_0 \otimes \sigma_3$	charge density wave
$\vec{\Delta}_1^s$	$\vec{\mathcal{M}}_1^s = \vec{\tau} \otimes \sigma_0$	Ferromagnet
$\vec{\Delta}_2^s$	$\vec{\mathcal{M}}_2^s = \vec{\tau} \otimes \sigma_1$	x -spin-current
$\vec{\Delta}_3^s$	$\vec{\mathcal{M}}_3^s = \vec{\tau} \otimes \sigma_2$	spin bond density
$\vec{\Delta}_4^s$	$\vec{\mathcal{M}}_4^s = \vec{\tau} \otimes \sigma_3$	AFM
Δ_1^{PP}	$\mathcal{M}_1^{\text{PP}} = \tau_2 \otimes \sigma_3$	s-wave SC
Δ_2^{PP}	$\mathcal{M}_2^{\text{PP}} = \tau_2 \otimes \sigma_1$	chiral SC1
Δ_3^{PP}	$\mathcal{M}_3^{\text{PP}} = \tau_2 \otimes \sigma_0$	chiral SC2
Δ_4^{PP}	$\mathcal{M}_4^{\text{PP}} = \tau_{0,1,3} \otimes \sigma_2$	triplet SC

lowest-energy limit. As for Type-II-RFP, interaction parameters delineated in Fig. 3(c)-(e) share the same sign-change (unchange) information with Type-I-RFP. In a sharp contrast to the other two types, it is of remarkable importance to emphasize that interaction parameters in the Type-II-Region approximately increase or decrease monotonically with the increase of η except some critical point. In addition to the difference of their concrete values, it is worth pointing out that the critical energy scales, at which RFPs are accessed, are nearly constants in Type-I-Region but instead proportional to η in both Type-II-Region and Type-III-Region.

Generally, the RFP with strong couplings is a significant impetus to trigger a multitude of unusual phenomena including instabilities and critical physical behaviors^{45,48,51,81–88}. Stimulated by these, we are going to investigate the potential instabilities around three distinct types of RFPs in the upcoming section and defer the underlying critical physical behaviors to Sec. V.

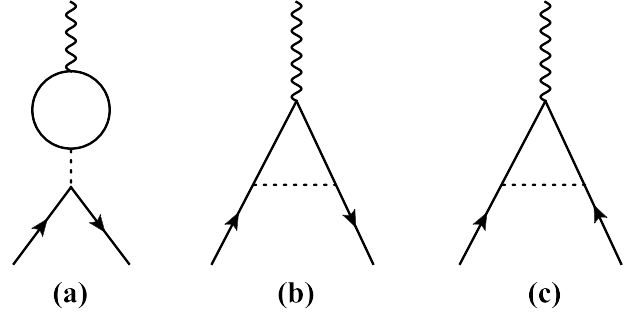


FIG. 6: One-loop corrections to the bilinear fermion-source terms^{48,51}: (a) and (b) represent the particle-hole channel and (c) specifies particle-particle channel. The solid, dash, and wave lines correspond to the fermion, fermion-fermion interaction and source term fields, respectively.

IV. INSTABILITIES INDUCED BY FERMION-FERMION INTERACTIONS

With the variation of structural coefficient η , we have confirmed in previous section there exist three distinct types (regions) of RFPs attesting to the subtle fermion-fermion interactions. As mentioned previously, instabilities are tightly linked to these RFPs, which are well-known signatures of symmetry breaking^{11,47,48,51,81–88,105}. In this respect, it is of enormous interest to seek and identify the leading instability and its related phase transition.

In order to justify potential types of symmetry breaking, we are suggested to bring out the following source terms that collect both the charge and spin channels^{11,45,48,106}

$$S_{\text{sou}} = \int d\tau \int d^2\mathbf{x} \sum_{i=1}^4 (\Delta_i^c \Psi^\dagger \mathcal{M}_i^c \Psi + \vec{\Delta}_i^s \cdot \Psi^\dagger \vec{\mathcal{M}}_i^s \Psi) + \int d\tau \int d^2\mathbf{x} \sum_{i=1}^4 (\Delta_i^{\text{PP}} \Psi^\dagger \mathcal{M}_i^{\text{PP}} \Psi^* + \text{H.c.}) \quad (12)$$

Hereby, the vertex matrixes $\mathcal{M}_i^{c/s}$ with $i = 1, 2, 3, 4$ denote various sorts of fermionic bilinears in the particle-hole part consisting of both charge and spin channels. In comparison, $\mathcal{M}_i^{\text{PP}}$ corresponds to possible fermionic bilinears in the particle-particle situation^{45,48}. In addition, the couplings $\Delta_i^{c/s}$ and Δ_i^{PP} serve as the strength of associated fermion-source terms, which can be regarded as order parameters accompanied by corresponding symmetry breakings. In principle, the onset of fermionic bilinear is a manifest signal for certain instability and hence implies a phase transition tied to some symmetry breaking^{47,81,84,85,105,107}. Table II catalogues the primary candidates of fermion bilinears and related phase transitions for our system.

A question is then naturally raised, which instability is the dominant one around three different types of RFPs. To elucidate this, we need to add the source terms (12)

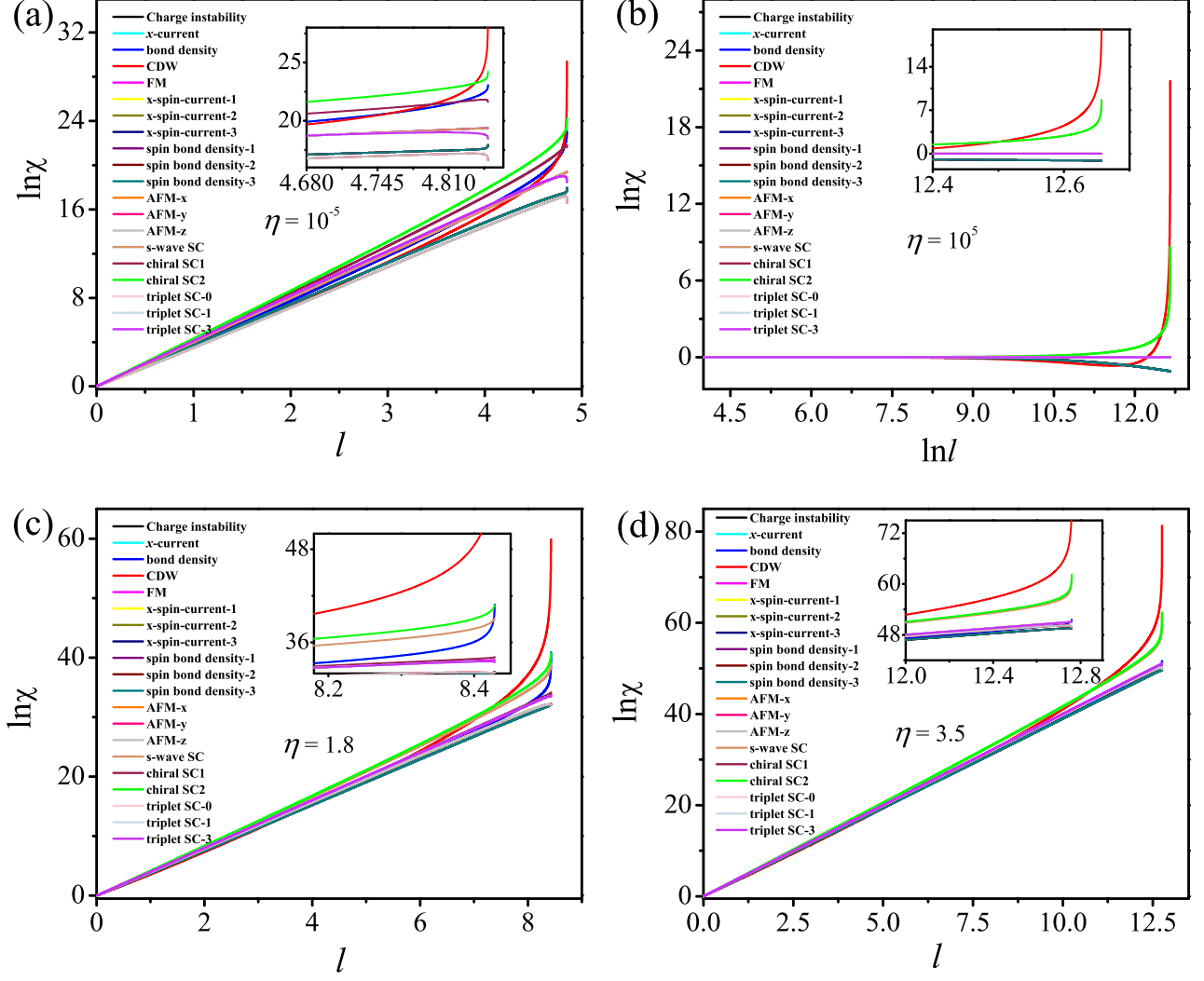


FIG. 7: (Color online) Flows of all particle-hole and particle-particle susceptibilities catalogued in Table II as functions of the RG evolution parameter l by approaching distinct types of RFPs classified and illustrated in Fig. 4 and Fig. 5. The x -spin-current- i and spin bond density- i with $i = 1, 2, 3$ as well as triplet SC- j with $j = 0, 1, 3$ and AFM- ζ with $\zeta = x, y, z$ are employed to specify distinct components of corresponding states as detailedly shown in Table II.

into our effective model. In this sense, the parameters Δ_i are entangled with the fermion-fermion interactions by virtue of efficiently receiving one-loop fermion-fermion corrections as diagrammatically illustrated in Fig. 6. After carrying out analogous procedures in Sec. II B^{45,48}, we notice that the strength of source term would be sensitive to energy scales and subject to the following set of RG evolutions

$$\frac{d\Delta_i^{c/s,PP}}{dl} = \mathcal{G}_i^{c/s,PP} \Delta_i^{c/s,PP}, \quad (13)$$

where the index i runs from 1 to 4 and the coefficients $\mathcal{G}_i^{c/s,PP}$ are closely dependent upon the fermion-fermion interactions plus structural parameters d_1 and d_3 . The details for the flows of source terms and coefficients $\mathcal{G}_i^{c/s,PP}$ are stored in Appendix C.

To proceed, we are capable of capturing the corresponding susceptibilities around the RFPs by adopting the relationship^{45,48}

$$\delta\chi = -\frac{\partial^2 \delta f}{\partial \Delta(0) \partial \Delta^*(0)}, \quad (14)$$

with f being the free energy density. Concerning the ground state can be characterized by the susceptibility with the strongest divergence^{11,47,48,51,81–88,105,108}, we are now in a suitable position to identify the very dominant instability and the associated phase transition nearby the corresponding RFP by computing and comparing the susceptibilities of all underlying instabilities listed in Table II.

To this end, we are forced to combine the RG evolutions of fermion-fermion interactions (11) and energy-

dependent strengths of source terms (13) in conjunction with the connections between susceptibilities and source-term couplings. After implementing long but straightforward numerical analysis, we are eventually left with the energy-dependent susceptibilities of all potential instabilities, which carry the low-energy physical information and determine the fates of all sorts of possible instabilities nearby distinct types of RFPs as apparently displayed in Fig. 7.

Subsequently, we deliver the primary results covered in Fig. 7. At the first sight, we figure out that all kinds of susceptibilities are fairly susceptible to energy scales and climb up quickly with accessing any sorts of the potential RFPs. Especially, it is of peculiar interest to address that fermion-fermion interactions are rather in favor of charge density wave (CDW). On one hand, the CDW susceptibility manifestly dominates over all other types once the system is tuned towards the expected RFP. On the other, this result is qualitatively insensitive to η . In other words, this kind of susceptibility is inevitable to be the strongest one no matter which type (region) of RFP is approached. Consequently, we come to a conclusion that the leading instability is directly associated with the phase transition from QBCP semimetal to CDW state under the influence of fermion-fermion couplings in the 2D QBCP materials sited on the kagomé lattice without time-reversal symmetry. It is worth pointing out that this result is basically in agreement with recent works on analogous compounds^{109–112}. This suggests that the CDW state is another winner driven by fermion-fermion interactions in the 2D QBCP materials besides quantum anomalous Hall and quantum spin Hall states in its checkerboard-lattice counterpart with time-reversal symmetry^{48,51}.

Next, we move to consider the subleading instability. Unlike the leading instability, we learning from Fig. 7 find that the subleading instabilities are of close relevance to the structural coefficient η and exhibit diverse fates in the vicinity of three different types of RFPs. To be concrete, as depicted in Fig. 7(a), susceptibilities of x -current, bond density, and chiral SC-2 are increased and become subdominant nearby Type-I-RFP. With respect to Type-II-RFP, the tendencies of all instabilities share the basic fates with Type-I-RFP once η is small. However, while η is increased to 1.8, the susceptibility of s-wave SC illustrated in Fig. 7(c) becomes comparable with that of x -current, bond density, and chiral SC-2 and thus can be regarded as another subleading instability. Further, s-wave SC and chiral SC-2 are gradually enhanced with the continue increase of η as delineated in Fig. 7(d) and become only two subdominant ones via eliminating x -current and bond density at $\eta = 3.5$. As for Type-III-RFP, Fig. 7(b) indicates that the qualitative results are analogous to Type-II-RFP's at $\eta = 3.5$, namely s-wave SC and chiral SC-2 are subleading phases. At last, it is notable to highlight that the critical energy scale dubbed l_c is rapidly increased (i.e. E_c is rapidly decreased) with tuning up the value of η . This means

that an enhancement of η is harmful to the emergence of instability.

To be brief, the dominant instability driven by fermion-fermion interactions is always tied to the CDW state irrespective of the value of η . In contrast, there exist four η -dependent candidates including the x -current and bond density as well as chiral SC-2 plus s-wave SC that are subordinate to the CDW state. Especially, we realize that the chiral SC-2 state is always subleading irrespective of concrete value of η . Rather, both the x -current and bond density can only play a subdominant role at a weak η . As the η is progressively increased, they share the positions with and eventually are replaced by the s-wave SC. Albeit the dominant instability generally takes a major responsibility for the low-energy physics, these subdominant ones might be in charge of related phenomena while the system is impacted by unexpected facets. For the sake of completeness, we are about to investigate how the behaviors of physical quantities are affected by the leading instability in the forthcoming section.

V. CRITICAL PHYSICAL IMPLICATIONS

On the basis of intimate fermion-fermion interactions in the low-energy sector, we have presented potential instabilities induced by fermionic interactions and corroborated in Sec. IV a direct connection between the overarching instability and CDW phase transition at certain RFP. At this stage, the RFP is tantamount to a phase transition point, at which the fluctuations are always so ferocious that usually render a plenty of singular critical behaviors^{90,113–118}. Accordingly, it is considerably fascinating and imperative to investigate possible physical implications triggered by the onset of CDW state.

Without loss of generality, we within this section put our focus on the density of states (DOS) as well as specific heat and compressibility of quasiparticles. In order to facilitate our study, we herein only concern with the qualitative criticality of these physical observables provoked by the dominant instability. To this end, our strategy is to introduce an order parameter Δ by hand⁷², which carries the main physical information of instability. Then adding it to Eq. (6), the free fermionic propagator dressed by one-loop corrections around the phase transition point is thus recast as

$$G_0(i\omega_n, \mathbf{k}) = \left(-i\omega_n + (d_3\mathbf{k}^2 + \Delta)\Sigma_{03} + d_1\Sigma_{01}(k_x^2 - k_y^2) + d_2\Sigma_{02}k_xk_y \right)^{-1}, \quad (15)$$

where $\omega_n = (2n + 1)\pi T$ with n being an integer stands for the Matsubara frequency. To proceed, performing analytical continuation $i\omega_n \rightarrow \omega_n + i\delta$, we are subsequently left with the retarded fermion propagator as follows¹¹⁸,

$$G_0^{\text{ret}}(\omega_n, \mathbf{k}) = \frac{(\omega_n + i\delta) + (d_3 k^2 + \Delta)\Sigma_{03} + d_1 k^2(\cos 2\theta\Sigma_{01} + \sin 2\theta\Sigma_{02})}{(-\omega_n^2 - 2i\omega_n\delta + d_3^2 k^4 + 2d_3 k^2\Delta + \Delta^2 + d_1^2 k^4)}. \quad (16)$$

We hereafter endeavor to extract the qualitative effects sparked by the formation of order parameter on the physical quantities one by one.

A. DOS

At first, let us concentrate on the DOS. For this purpose, one necessitates the corresponding spectral function, which is directly connected to the retarded fermion propagator (16)^{89,118} and of the following form

$$\begin{aligned} \mathcal{A}(\omega_n, \mathbf{k}) &= -\frac{1}{\pi} \text{Tr} (\text{Im} G_0^{\text{ret}}(\omega_n, \mathbf{k})) \\ &= 4N |\omega_n| \delta(d_3^2 k^4 + 2d_3 k^2 \Delta + \Delta^2 + d_1^2 k^4 - \omega_n^2), \end{aligned} \quad (17)$$

where the number N characterizes the fermion flavor. With this respect, the DOS of quasiparticles consequently can be casted as

$$\rho(\omega_n) = N \int_0^{\Lambda_0} \int_0^{2\pi} \frac{k dk d\theta}{(2\pi)^2} \mathcal{A}(\omega_n, \mathbf{k}). \quad (18)$$

Prior to inspecting the impact of order parameter, it is necessary to briefly discuss the circumstance in the absence of instability. Taking $\Delta \rightarrow 0$ limit in Eq. (18) directly gives rise to

$$\rho(\omega_n) = \frac{N}{2\pi \sqrt{d_3^2 + d_1^2}}. \quad (19)$$

This is in reminiscence of the fact that the DOS of 2D QBCP system is a finite constant at the Fermi surface^{44,48}.

Subsequently, we go to examine the very influence of order parameter. Based upon the general result (18) in tandem with the essential properties of δ function, we notice that the DOS would be broken down into two distinct situations depending upon Δ 's magnitude. On one hand, one can find the ω_n or temperature (T) dependence of DOS at $|\Delta| < T$ is rewritten as follows

$$\rho(\omega_n) = \frac{N}{2\pi \sqrt{d_3^2 + d_1^2 (1 - \frac{\Delta^2}{\omega_n^2})}}. \quad (20)$$

On the other hand, a large order parameter with $|\Delta| > T$ is of particular detrimental to DOS which disappears exactly at the instability, namely

$$\rho(\omega_n) = 0. \quad (21)$$

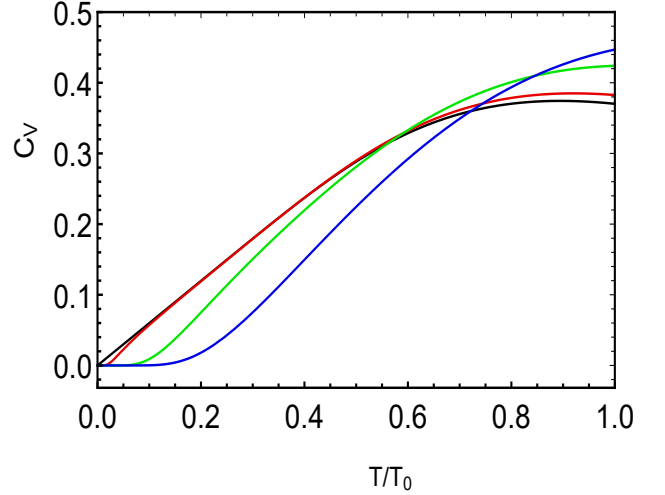


FIG. 8: (Color online) Temperature dependence of the specific heat C_V accessing the Type-II-RFP under the CDW fluctuation. The black, red, green, and blue lines correspond to $\Delta' = 0$, $\Delta' = 0.1$, $\Delta' = 0.5$, and $\Delta' = 1$, respectively (the qualitative results for Type-I-RFP are analogous and hence not shown here).

These manifestly shed light on the importance of order parameter in the proximity of instability. Compared to a finite constant for 2D QBCP materials with $\Delta = 0$, we figure out that the DOS nearby Fermi surface (QBCP) is slightly enhanced while the system is a little far away from instability with $|\Delta| < T$. In addition, its concrete values as clearly designated in Eqs. (19)-(20) are heavily dependent upon two microscopic parameters d_3 and d_1 , which are closely associated with different types of RFPs. However, once the RFP is sufficiently approached with $|\Delta| > T$, the onset of large order parameter substantially suppresses the DOS due to ferocious fluctuations. In other words, the band structure of 2D QBCP systems would be completely sabotaged^{52,82}. It is worth emphasizing that we have checked all sorts of RFPs share the analogous qualitative results.

B. Specific heat

Next, we are going to shift our target to the specific heat of quasiparticles. For the sake of completeness, we hereby bring out an infinitesimal chemical potential μ into our effective theory^{89,119}. As a result, the corresponding free fermionic propagator in the Matsubara formalism is reformulated into

$$G_0(i\omega_n, \mathbf{k}) = \frac{1}{i\omega_n + \mu - \mathcal{H}_0(k) - \Delta\Sigma_{03}} = -\frac{i\omega_n + \mu + (d_3k^2 + \Delta)\Sigma_{03} + d_1\Sigma_{01}k^2 \cos 2\theta + d_1\Sigma_{02}k^2 \sin 2\theta}{(\omega_n - i\mu)^2 + (d_3k^2 + \Delta)^2 + d_1^2k^4}. \quad (22)$$

Following the tactic in Ref.⁸⁹, we integrate over all frequencies and then write the free energy of the fermions as

$$f(T, \mu) = -2N \sum_{\alpha \pm 1} \int \frac{d^2\mathbf{k}}{(2\pi)^2} \left[\epsilon(\mathbf{k}) + T \ln \left(1 + e^{-\frac{\epsilon(\mathbf{k}) + \alpha\mu}{T}} \right) \right], \quad (23)$$

where the energy is nominated as

$$\epsilon(\mathbf{k}) \equiv \sqrt{(d_3\mathbf{k}^2 + \Delta)^2 + d_1^2\mathbf{k}^4}. \quad (24)$$

To simplify our study, we take advantage of transformation $f(T) - f(0) \rightarrow f(T)$ to eliminate the zero-point energy and obtain a compact free energy as follows

$$f(T, \mu) = -2NT \sum_{\alpha \pm 1} \int_0^{\Lambda_0} \int_0^{2\pi} \frac{kdkd\theta}{(2\pi)^2} \ln \left(1 + e^{-\frac{\epsilon(\mathbf{k}) + \alpha\mu}{T}} \right). \quad (25)$$

In this sense, we hereafter only pour our attention into $\mu = 0$ situation for specific heat, which is based upon two points. On one side, the starting point (5) is restricted to zero chemical potential at the QBCP. On the other side, this work only concerns qualitative phenomena of physical implications triggered by an instability irrespective of the value of μ . To proceed, supposing $\mu = 0$ in Eq. (25) gives rise to

$$f(T) = -4NT \int_0^{\Lambda_0} \int_0^{2\pi} \frac{kdkd\theta}{(2\pi)^2} \ln \left(1 + e^{-\frac{\epsilon(\mathbf{k})}{T}} \right). \quad (26)$$

Taking the derivatives of free energy with respect to temperature forthrightly yields to the specific heat (C_V)^{89,119}

$$C_V(T) = -T \frac{\partial^2 f(T)}{\partial T^2} = \frac{2N}{\pi T^2} \int_0^{\Lambda_0} \frac{kdk \epsilon^2(\mathbf{k}) e^{-\frac{\epsilon(\mathbf{k})}{T}}}{\left(e^{-\frac{\epsilon(\mathbf{k})}{T}} + 1 \right)^2}. \quad (27)$$

In order to facilitate our calculations, it is convenient to rescale the momentum and order parameter with the cutoff temperature T_0 that is related to the cutoff Λ_0 by $T_0 \equiv \Lambda_0^2$, namely $k' \equiv k/\sqrt{T_0}$ and $\Delta' \equiv \Delta/T_0$ ⁸⁹. As a corollary, we can convert the $C_V(T)$ into the following form

$$C_V(T) = \frac{2NT_0^3}{\pi T^2} \int_0^1 \frac{k' dk' \epsilon'^2(\mathbf{k}', \Delta') e^{-\frac{\epsilon'(\mathbf{k}', \Delta')}{T/T_0}}}{\left(e^{-\frac{\epsilon'(\mathbf{k}', \Delta')}{T/T_0}} + 1 \right)^2}, \quad (28)$$

where the ϵ' is designated as

$$\epsilon'(\mathbf{k}', \Delta') \equiv \sqrt{(d_3k'^2 + \Delta')^2 + d_1^2k'^4}. \quad (29)$$

On the basis of the general expression for $C_V(T)$ (28), a few comments on the specific heat are addressed under the influence of an order parameter kindled by the CDW instability. We at first tackle the limit case with $\Delta' = 0$ (i.e., the 2D QBCP state). In this circumstance, it is fortunate that the analytical result (28) can be obtained by integrating out the momenta

$$C_V(T) = \frac{2NT_0^{\frac{3}{2}}}{\pi\sqrt{T}} \frac{\left[6 \frac{(d_3^2 + d_1^2)}{(T/T_0)^2} \frac{e^{-\frac{\sqrt{d_3^2 + d_1^2}}{T/T_0}}}{1 + e^{-\frac{\sqrt{d_3^2 + d_1^2}}{T/T_0}}} - 12 \frac{\sqrt{d_3^2 + d_1^2}}{T/T_0} \log \left(1 + e^{-\frac{\sqrt{d_3^2 + d_1^2}}{T/T_0}} \right) - 12 \text{Li}_2 \left(-e^{-\frac{\sqrt{d_3^2 + d_1^2}}{T/T_0}} \right) - \pi^2 \right]}{12(d_3^2 + d_1^2)^{\frac{1}{2}}}, \quad (30)$$

with $\text{Li}_2(z)$ corresponding to a polylogarithmic function¹²⁰. This will be utilized to compare with its $\Delta' \neq 0$ counterparts.

Subsequently, we endeavor to investigate the nontrivial situation with a moderate order parameter once the system is adjacent to RFP (not exactly accessed). Carrying out the numerical analysis of Eqs. (28) and (30) yields several interesting features shown in Fig. 8 and Fig. 9. Studying from Fig. 8, one broadly realizes that the fates of $C_V(T)$ around Type-II-RFP are fairly dependent upon Δ' (the qualitative result for Type-I-RFP is analo-

gous and thus not shown here). In the low-temperature region, the order parameter apparently hampers the specific heat. On the contrary, C_V gains a slight lift in the high-temperature region. In comparison, Fig. 9 displays that Δ' always brings some detriments to C_V as the system is close to the Type-III-RFP. Eventually, we examine the limit $\Delta' \gg 1$ (namely $\Delta \gg T_0$), which would be ignited once the RFP is approached. In this respect, combining Eq. (28) with this limit is expected to grasp

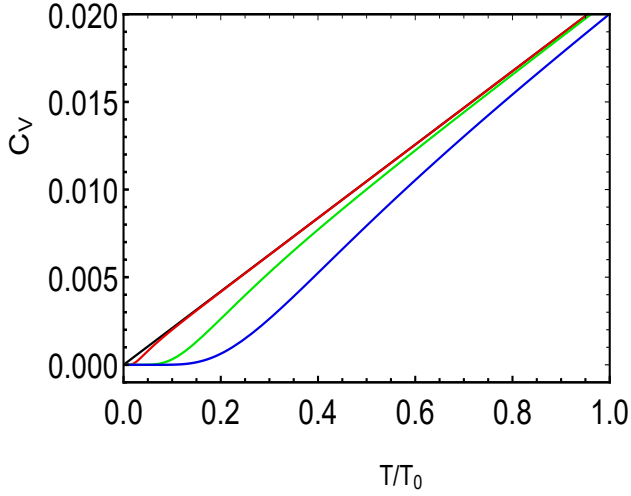


FIG. 9: (Color online) Temperature dependence of the specific heat C_V approaching the Type-III-RFP under the CDW fluctuation. The black, red, green, and blue lines correspond to $\Delta' = 0$, $\Delta' = 0.1$, $\Delta' = 0.5$, and $\Delta' = 1$, respectively.

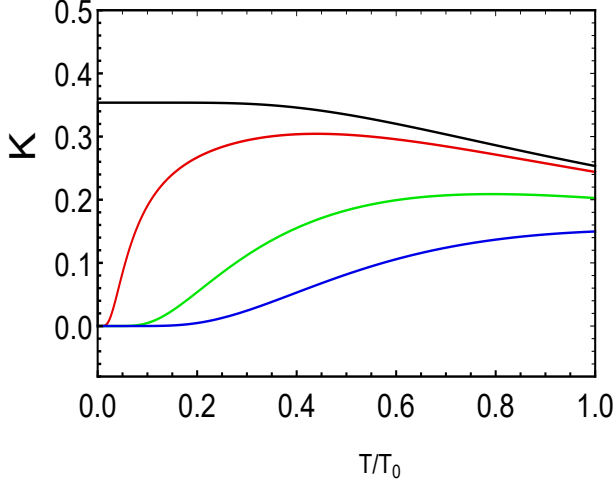


FIG. 10: (Color online) Temperature dependence of the compressibility κ approaching the Type-II-RFP under the CDW fluctuation. The black, red, green, and blue lines correspond to $\Delta' = 0$, $\Delta' = 0.1$, $\Delta' = 0.5$, and $\Delta' = 1$, respectively (the basic conclusions for both Type-I-RFP and Type-III-RFP are similar and hence not shown here).

the central point of specific heat

$$C_V(T) \approx \frac{NT_0^3 \Delta'^2}{\pi T^2 e^{\frac{\Delta'}{T/T_0}}}, \quad (31)$$

which signals $\lim_{\Delta' \rightarrow \infty} C_V(T) \rightarrow 0$. It manifestly indicates that C_V is profoundly reduced at the CDW instability.

C. Compressibility

At last, with the help of temperature- and μ -dependent free energy derived in Eq. (25), we are allowed to verify how the compressibility of quasiparticles labeled by κ behaves in the proximity of the leading instability. Concretely, the temperature dependence of κ reads^{89,121–123}

$$\kappa(T) = - \left. \frac{\partial^2 f(T, \mu)}{\partial \mu^2} \right|_{\mu=0} = \frac{2N}{\pi T} \int_0^{\Lambda_0} k dk \frac{e^{\frac{\epsilon(\mathbf{k})}{T}}}{\left(e^{\frac{\epsilon(\mathbf{k})}{T}} + 1\right)^2}, \quad (32)$$

with $\epsilon(\mathbf{k})$ being denominated in Eq. (24) for the absence of chemical potential. We then adopt the same rescalings employed in Sec. VB and are left with

$$\kappa(T) = \frac{2N}{\pi(T/T_0)} \int_0^1 k' dk' \frac{e^{\frac{\epsilon'(\mathbf{k}', \Delta')}{T/T_0}}}{\left(e^{\frac{\epsilon'(\mathbf{k}', \Delta')}{T/T_0}} + 1\right)^2}, \quad (33)$$

where $\epsilon'(\mathbf{k}', \Delta')$ is designated in Eq. (29).

Accordingly, the analytical expressions for $\Delta' = 0$ and $\Delta' \gg 1$ can also be easily obtained,

$$\kappa(T, \Delta' = 0) = \frac{N \tanh\left(\frac{\sqrt{d_3^2 + d_1^2}}{2(T/T_0)}\right)}{2\pi \sqrt{d_3^2 + d_1^2}}, \quad (34)$$

$$\kappa(T, \Delta' \gg 1) \approx \frac{N}{\pi(T/T_0)} e^{-\frac{\Delta'}{T/T_0}}. \quad (35)$$

Numerically implementing Eq. (33) leads to Fig. 10, which implies that the compressibility is severely suppressed by a finite order parameter. Additionally, Eq. (35) proposes that the compressibility goes toward vanishment because of the divergent fluctuation of order parameter exactly at the RFP. It is worth emphasizing that all these basic conclusions are insensitive to concrete values of RFP. In such circumstances, we would like to assume this phenomenon to be the third critical behavior driven by fermion-fermion interactions^{82,89}.

VI. SUMMARY

In summary, we attentively verify how the low-energy properties of 2D spin-1/2 QBCP fermionic systems on the kagomé lattice are impacted by all sixteen sorts of marginal fermion-fermion interactions. For the purpose of treating these degrees of freedom on the same footing, we resort to the momentum-shell RG method^{78–80}, which is a well-trodden strategy for the description of hierarchical physics under the simultaneous coexistence of multiple sorts of interactions. In the spirit of standard RG analysis, a set of coupled flow equations of all interaction strengths are derived by taking into account

one-loop corrections of the correlated Feynman diagrams. After vigilantly analyzing these RG evolutions, several fascinating behaviors ignited by fermion-fermion interactions are addressed in the low-energy sector.

At first, we notice that some sorts of fermion-fermion couplings coalesce with the decrease of energy scale due to their intimate correlations. This tenders just six of them can flow independently and evolve divergently with lowering energy scales. In this respect, we only need to contemplate the energy-dependent trajectories of six non-trivial fermionic couplings. In order to work in the perturbative theory, it is convenient to rescale these strong-coupling interactions with a non-sign changed parameters (such as λ_{30}) and obtain the relative flows of interaction parameters as well as their RFPs that directly govern the critical physics^{45,48,51}. In particular, these RFPs are of close association with the coefficient composed by two structure parameters (i.e., $\eta \equiv d_3/d_1$). To be concrete, Fig. 4 and Fig. 5 unambiguously manifest three qualitatively distinct η -dependent regions, which are named as Type-I-Region, Type-II-Region, and Type-III-Region residing in $\eta < C_1$, $C_1 < \eta < C_2$, and $\eta > C_2$, respectively. Focusing on the vicinity of RFPs in these three different regions, we then carefully investigate the underlying instabilities, which are accompanied by corresponding symmetry breakings and tied to related phase transitions^{47,48,51,81–88}. On the basis of numerical RG studies together with comparisons of susceptibilities, we, reading off Fig. 7, draw a conclusion that the CDW instability is always dominant over all other candidates irrespective of the specific value of η . In contrast, four subleading ones are also manifestly proposed, which in-

clude x -current, bond density, chiral SC-2, and s-wave SC depending upon the variation of η . Furthermore, we finally examine the critical fates of physical implications consisting of DOS and specific heat as well as compressibility nearby the dominant instability, namely the phase transition from a QBCP semimetal to CDW state. To be specific, the development of CDW state is very harmful to these three kinds of physical observables as displayed in Figs. 8-10. Especially, they are all considerably suppressed and even vanish once the instability is divergent with a sufficiently large order parameter. These results are reminiscent of quantum critical behaviors in the low-energy regime^{90,113–118}.

We wish these studies would supplement current understandings of 2D QBCP semimetals and open helpful routes to promote further research of 2D QBCP materials as well as explore their cousin materials in the future.

ACKNOWLEDGEMENTS

J.W. is partially supported by the National Natural Science Foundation of China under Grant No. 11504360. The authors would like to thank Jie-Qiong Li, Xiao-Yue Ren, and Yao-Ming Dong for helpful discussions.

Appendix A: One-loop corrections

The one-loop corrections to self-energy and fermion-fermion interactions are depicted in Fig. 11. After long but straightforward calculations, we obtain^{48,51}

$$S_{00} = - \int_{-\infty}^{\infty} \frac{d\omega_1 d\omega_2 d\omega_3}{(2\pi)^3} \int \frac{d^2 \mathbf{k}_1 d^2 \mathbf{k}_2 d^2 \mathbf{k}_3}{(2\pi)^6} \Psi^\dagger(\omega_1, \mathbf{k}_1) \Sigma_{00} \Psi(\omega_2, \mathbf{k}_2) \Psi^\dagger(\omega_3, \mathbf{k}_3) \Sigma_{00} \Psi(\omega_1 + \omega_2 - \omega_3, \mathbf{k}_1 + \mathbf{k}_2 - \mathbf{k}_3) \\ \times [2d_3^2(\lambda_{00}\lambda_{03} + \lambda_{10}\lambda_{13} + \lambda_{20}\lambda_{23} + \lambda_{30}\lambda_{33}) + d_1^2(\lambda_{00}\lambda_{01} + \lambda_{10}\lambda_{11} + \lambda_{20}\lambda_{21} + \lambda_{30}\lambda_{31} + \lambda_{00}\lambda_{02} + \lambda_{10}\lambda_{12} + \lambda_{20}\lambda_{22} \\ + \lambda_{30}\lambda_{32})] \frac{l}{4\pi(d_3^2 + d_1^2)^{\frac{3}{2}}}, \quad (A1)$$

$$S_{10} = \int_{-\infty}^{\infty} \frac{d\omega_1 d\omega_2 d\omega_3}{(2\pi)^3} \int \frac{d^2 \mathbf{k}_1 d^2 \mathbf{k}_2 d^2 \mathbf{k}_3}{(2\pi)^6} \Psi^\dagger(\omega_1, \mathbf{k}_1) \Sigma_{10} \Psi(\omega_2, \mathbf{k}_2) \Psi^\dagger(\omega_3, \mathbf{k}_3) \Sigma_{10} \Psi(\omega_1 + \omega_2 - \omega_3, \mathbf{k}_1 + \mathbf{k}_2 - \mathbf{k}_3) \\ \times \{2d_3^2[\lambda_{20}\lambda_{30} + \lambda_{21}\lambda_{31} + \lambda_{22}\lambda_{32} + \lambda_{23}\lambda_{33} - (\lambda_{13}\lambda_{00} + \lambda_{10}\lambda_{03} + \lambda_{21}\lambda_{32} + \lambda_{22}\lambda_{31})] + d_1^2[2(\lambda_{20}\lambda_{30} + \lambda_{21}\lambda_{31} \\ + \lambda_{22}\lambda_{32} + \lambda_{23}\lambda_{33}) - (\lambda_{01}\lambda_{10} + \lambda_{00}\lambda_{11} + \lambda_{22}\lambda_{33} + \lambda_{23}\lambda_{32} + \lambda_{12}\lambda_{00} + \lambda_{10}\lambda_{02} + \lambda_{23}\lambda_{31} + \lambda_{21}\lambda_{33})]\} \frac{l}{4\pi(d_3^2 + d_1^2)^{\frac{3}{2}}}, \quad (A2)$$

$$S_{20} = \int_{-\infty}^{\infty} \frac{d\omega_1 d\omega_2 d\omega_3}{(2\pi)^3} \int \frac{d^2 \mathbf{k}_1 d^2 \mathbf{k}_2 d^2 \mathbf{k}_3}{(2\pi)^6} \Psi^\dagger(\omega_1, \mathbf{k}_1) \Sigma_{20} \Psi(\omega_2, \mathbf{k}_2) \Psi^\dagger(\omega_3, \mathbf{k}_3) \Sigma_{20} \Psi(\omega_1 + \omega_2 - \omega_3, \mathbf{k}_1 + \mathbf{k}_2 - \mathbf{k}_3) \\ \times \{2d_3^2[\lambda_{30}\lambda_{10} + \lambda_{31}\lambda_{11} + \lambda_{32}\lambda_{12} + \lambda_{33}\lambda_{13} - (\lambda_{23}\lambda_{00} + \lambda_{20}\lambda_{03} + \lambda_{31}\lambda_{12} + \lambda_{32}\lambda_{11})] + d_1^2[2(\lambda_{30}\lambda_{10} + \lambda_{31}\lambda_{11} \\ + \lambda_{32}\lambda_{12} + \lambda_{33}\lambda_{13}) - (\lambda_{21}\lambda_{00} + \lambda_{20}\lambda_{01} + \lambda_{32}\lambda_{13} + \lambda_{33}\lambda_{12} + \lambda_{22}\lambda_{00} + \lambda_{20}\lambda_{02} + \lambda_{33}\lambda_{11} + \lambda_{31}\lambda_{13})]\} \frac{l}{4\pi(d_3^2 + d_1^2)^{\frac{3}{2}}}, \quad (A3)$$

$$S_{30} = \int_{-\infty}^{\infty} \frac{d\omega_1 d\omega_2 d\omega_3}{(2\pi)^3} \int \frac{d^2 \mathbf{k}_1 d^2 \mathbf{k}_2 d^2 \mathbf{k}_3}{(2\pi)^6} \Psi^\dagger(\omega_1, \mathbf{k}_1) \Sigma_{30} \Psi(\omega_2, \mathbf{k}_2) \Psi^\dagger(\omega_3, \mathbf{k}_3) \Sigma_{30} \Psi(\omega_1 + \omega_2 - \omega_3, \mathbf{k}_1 + \mathbf{k}_2 - \mathbf{k}_3) \\ \times \{2d_3^2[\lambda_{10}\lambda_{20} + \lambda_{11}\lambda_{21} + \lambda_{12}\lambda_{22} + \lambda_{13}\lambda_{23} - (\lambda_{33}\lambda_{00} + \lambda_{30}\lambda_{03} + \lambda_{11}\lambda_{22} + \lambda_{12}\lambda_{21})] + d_1^2[2(\lambda_{10}\lambda_{20} + \lambda_{11}\lambda_{21}$$

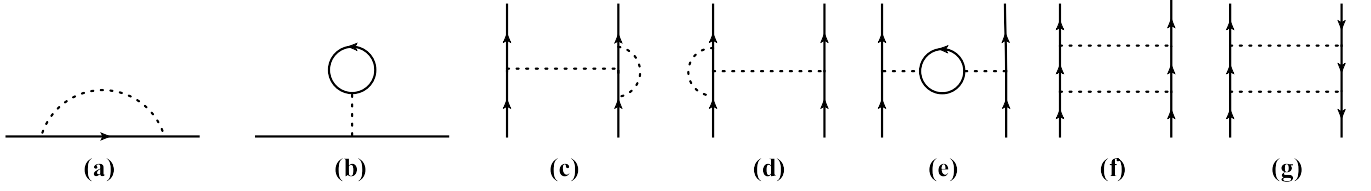


FIG. 11: One-loop corrections to (a)-(b): the fermion propagator and (c)-(g): the fermion-fermion interactions. The solid and dashed lines characterize the fermion propagator and four-fermion interactions, respectively^{48,51}.

Appendix B: RG flow equations of all interaction parameters

Combining our effective action (5) and the RG rescalings (7)-(10) as well as all the one-loop corrections presented in Appendix A, we consequently are left with the following coupled RG evolutions of fermion-fermion interactions after carrying out the standard procedures of RG analysis^{48,95,97,98}

$$\frac{d\lambda_{00}}{dl} = -\frac{1}{4\pi(d_3^2 + d_1^2)^{\frac{3}{2}}} [2d_3^2(\lambda_{00}\lambda_{03} + \lambda_{10}\lambda_{13} + \lambda_{20}\lambda_{23} + \lambda_{30}\lambda_{33}) + d_1^2(\lambda_{00}\lambda_{01} + \lambda_{10}\lambda_{11} + \lambda_{20}\lambda_{21} + \lambda_{30}\lambda_{31} + \lambda_{00}\lambda_{02} + \lambda_{10}\lambda_{12} + \lambda_{20}\lambda_{22} + \lambda_{30}\lambda_{32})], \quad (B1)$$

$$\frac{d\lambda_{10}}{dl} = \frac{1}{4\pi(d_3^2 + d_1^2)^{\frac{3}{2}}} [2d_3^2[\lambda_{20}\lambda_{30} + \lambda_{21}\lambda_{31} + \lambda_{22}\lambda_{32} + \lambda_{23}\lambda_{33} - (\lambda_{13}\lambda_{00} + \lambda_{10}\lambda_{03} + \lambda_{21}\lambda_{32} + \lambda_{22}\lambda_{31})] + d_1^2[2(\lambda_{20}\lambda_{30} + \lambda_{21}\lambda_{31} + \lambda_{22}\lambda_{32} + \lambda_{23}\lambda_{33}) - (\lambda_{01}\lambda_{10} + \lambda_{00}\lambda_{11} + \lambda_{22}\lambda_{33} + \lambda_{23}\lambda_{32} + \lambda_{12}\lambda_{00} + \lambda_{10}\lambda_{02} + \lambda_{23}\lambda_{31} + \lambda_{21}\lambda_{33})]], \quad (B2)$$

$$\frac{d\lambda_{20}}{dl} = \frac{1}{4\pi(d_3^2 + d_1^2)^{\frac{3}{2}}} [2d_3^2[\lambda_{30}\lambda_{10} + \lambda_{31}\lambda_{11} + \lambda_{32}\lambda_{12} + \lambda_{33}\lambda_{13} - (\lambda_{23}\lambda_{00} + \lambda_{20}\lambda_{03} + \lambda_{31}\lambda_{12} + \lambda_{32}\lambda_{11})] + d_1^2[2(\lambda_{30}\lambda_{10} + \lambda_{31}\lambda_{11} + \lambda_{32}\lambda_{12} + \lambda_{33}\lambda_{13}) - (\lambda_{21}\lambda_{00} + \lambda_{20}\lambda_{01} + \lambda_{32}\lambda_{13} + \lambda_{33}\lambda_{12} + \lambda_{22}\lambda_{00} + \lambda_{20}\lambda_{02} + \lambda_{33}\lambda_{11} + \lambda_{31}\lambda_{13})]], \quad (B3)$$

$$\frac{d\lambda_{30}}{dl} = \frac{1}{4\pi(d_3^2 + d_1^2)^{\frac{3}{2}}} [2d_3^2[\lambda_{10}\lambda_{20} + \lambda_{11}\lambda_{21} + \lambda_{12}\lambda_{22} + \lambda_{13}\lambda_{23} - (\lambda_{33}\lambda_{00} + \lambda_{30}\lambda_{03} + \lambda_{11}\lambda_{22} + \lambda_{12}\lambda_{21})] + d_1^2[2(\lambda_{10}\lambda_{20} + \lambda_{11}\lambda_{21} + \lambda_{12}\lambda_{22} + \lambda_{13}\lambda_{23}) - (\lambda_{31}\lambda_{00} + \lambda_{30}\lambda_{01} + \lambda_{12}\lambda_{23} + \lambda_{13}\lambda_{22} + \lambda_{32}\lambda_{00} + \lambda_{30}\lambda_{02} + \lambda_{13}\lambda_{21} + \lambda_{11}\lambda_{23})]], \quad (B4)$$

$$\frac{d\lambda_{01}}{dl} = \frac{1}{8\pi(d_3^2 + d_1^2)^{\frac{3}{2}}} \{4d_3^2[\lambda_{01}\lambda_{00} + \lambda_{01}\lambda_{10} + \lambda_{01}\lambda_{11} + \lambda_{01}\lambda_{20} + \lambda_{01}\lambda_{21} + \lambda_{01}\lambda_{30} + \lambda_{01}\lambda_{31} + \lambda_{03}\lambda_{02} + \lambda_{13}\lambda_{12} + \lambda_{23}\lambda_{22} + \lambda_{33}\lambda_{32} - (\lambda_{01}\lambda_{02} + \lambda_{01}\lambda_{03} + \lambda_{01}\lambda_{12} + \lambda_{01}\lambda_{13} + \lambda_{01}\lambda_{22} + \lambda_{01}\lambda_{23} + \lambda_{01}\lambda_{32} + \lambda_{01}\lambda_{33} + 3\lambda_{01}\lambda_{01} + \lambda_{02}\lambda_{00} + \lambda_{12}\lambda_{10} + \lambda_{22}\lambda_{20} + \lambda_{32}\lambda_{30})] + d_1^2[2(\lambda_{01}\lambda_{00} + \lambda_{01}\lambda_{10} + \lambda_{01}\lambda_{11} + \lambda_{01}\lambda_{20} + \lambda_{01}\lambda_{21} + \lambda_{01}\lambda_{30} + \lambda_{01}\lambda_{31}) + 4(\lambda_{03}\lambda_{02} + \lambda_{13}\lambda_{12} + \lambda_{23}\lambda_{22} + \lambda_{33}\lambda_{32}) - (\lambda_{00}\lambda_{00} + \lambda_{10}\lambda_{10} + \lambda_{20}\lambda_{20} + \lambda_{30}\lambda_{30} + \lambda_{01}\lambda_{01} + \lambda_{11}\lambda_{11} + \lambda_{21}\lambda_{21} + \lambda_{31}\lambda_{31} + \lambda_{02}\lambda_{02} + \lambda_{12}\lambda_{12} + \lambda_{22}\lambda_{22} + \lambda_{32}\lambda_{32} + \lambda_{03}\lambda_{03} + \lambda_{13}\lambda_{13} + \lambda_{23}\lambda_{23} + \lambda_{33}\lambda_{33}) - 2(\lambda_{01}\lambda_{02} + \lambda_{01}\lambda_{03} + \lambda_{01}\lambda_{12} + \lambda_{01}\lambda_{13} + \lambda_{01}\lambda_{22} + \lambda_{01}\lambda_{23} + \lambda_{01}\lambda_{32} + \lambda_{01}\lambda_{33} + 3\lambda_{01}\lambda_{01} + \lambda_{03}\lambda_{00} + \lambda_{13}\lambda_{10} + \lambda_{23}\lambda_{20} + \lambda_{33}\lambda_{30})]\}, \quad (B5)$$

$$\frac{d\lambda_{11}}{dl} = \frac{1}{4\pi(d_3^2 + d_1^2)^{\frac{3}{2}}} [2d_3^2[\lambda_{12}\lambda_{03} + \lambda_{13}\lambda_{02} + \lambda_{31}\lambda_{20} + \lambda_{30}\lambda_{21} + \lambda_{11}\lambda_{00} + \lambda_{11}\lambda_{01} + \lambda_{11}\lambda_{10} + \lambda_{11}\lambda_{22} + \lambda_{11}\lambda_{23} + \lambda_{11}\lambda_{32} + \lambda_{11}\lambda_{33} - (\lambda_{12}\lambda_{00} + \lambda_{10}\lambda_{02} + \lambda_{33}\lambda_{21} + \lambda_{31}\lambda_{23} + \lambda_{11}\lambda_{02} + \lambda_{11}\lambda_{03} + \lambda_{11}\lambda_{12} + \lambda_{11}\lambda_{13} + \lambda_{11}\lambda_{20} + \lambda_{11}\lambda_{21} + \lambda_{11}\lambda_{30} + \lambda_{11}\lambda_{31} + 3\lambda_{11}\lambda_{11})] + d_1^2[\lambda_{11}\lambda_{00} + \lambda_{11}\lambda_{01} + \lambda_{11}\lambda_{10} + \lambda_{11}\lambda_{22} + \lambda_{11}\lambda_{23} + \lambda_{11}\lambda_{32} + \lambda_{11}\lambda_{33} + 2(\lambda_{12}\lambda_{03} + \lambda_{13}\lambda_{02} + \lambda_{31}\lambda_{20} + \lambda_{30}\lambda_{21}) - (\lambda_{10}\lambda_{00} + \lambda_{11}\lambda_{01} + \lambda_{12}\lambda_{02} + \lambda_{13}\lambda_{03} + \lambda_{13}\lambda_{00} + \lambda_{10}\lambda_{03} + \lambda_{31}\lambda_{22} + \lambda_{32}\lambda_{21} + \lambda_{11}\lambda_{02} + \lambda_{11}\lambda_{03} + \lambda_{11}\lambda_{12} + \lambda_{11}\lambda_{13} + \lambda_{11}\lambda_{20} + \lambda_{11}\lambda_{21} + \lambda_{11}\lambda_{30} + \lambda_{11}\lambda_{31} + 3\lambda_{11}\lambda_{11})]], \quad (B6)$$

$$\frac{d\lambda_{21}}{dl} = \frac{1}{4\pi(d_3^2 + d_1^2)^{\frac{3}{2}}} [2d_3^2[\lambda_{22}\lambda_{03} + \lambda_{23}\lambda_{02} + \lambda_{11}\lambda_{30} + \lambda_{10}\lambda_{31} + \lambda_{21}\lambda_{00} + \lambda_{21}\lambda_{01} + \lambda_{21}\lambda_{12} + \lambda_{21}\lambda_{13} + \lambda_{21}\lambda_{20} + \lambda_{21}\lambda_{22} + \lambda_{21}\lambda_{23} - (\lambda_{22}\lambda_{00} + \lambda_{20}\lambda_{02} + \lambda_{13}\lambda_{31} + \lambda_{11}\lambda_{33} + \lambda_{21}\lambda_{02} + \lambda_{21}\lambda_{03} + \lambda_{21}\lambda_{10} + \lambda_{21}\lambda_{11} + \lambda_{21}\lambda_{22} + \lambda_{21}\lambda_{23} + \lambda_{21}\lambda_{30} + \lambda_{21}\lambda_{31} + 3\lambda_{21}\lambda_{21})] + d_1^2[2(\lambda_{22}\lambda_{03} + \lambda_{23}\lambda_{02} + \lambda_{11}\lambda_{30} + \lambda_{10}\lambda_{31}) + \lambda_{21}\lambda_{00} + \lambda_{21}\lambda_{01} + \lambda_{21}\lambda_{12} + \lambda_{21}\lambda_{13} + \lambda_{21}\lambda_{20} + \lambda_{21}\lambda_{21} + \lambda_{21}\lambda_{22} + \lambda_{21}\lambda_{23} - (\lambda_{20}\lambda_{00} + \lambda_{21}\lambda_{01} + \lambda_{22}\lambda_{02} + \lambda_{23}\lambda_{03} + \lambda_{23}\lambda_{00} + \lambda_{20}\lambda_{03} + \lambda_{11}\lambda_{32} + \lambda_{12}\lambda_{31} + \lambda_{21}\lambda_{02} + \lambda_{21}\lambda_{03} + \lambda_{21}\lambda_{10} + \lambda_{21}\lambda_{11} + \lambda_{21}\lambda_{22} + \lambda_{21}\lambda_{23} + \lambda_{21}\lambda_{30} + \lambda_{21}\lambda_{31} + 3\lambda_{21}\lambda_{21})]], \quad (B7)$$

$$+ \lambda_{30}\lambda_{02} + \lambda_{23}\lambda_{11} + \lambda_{21}\lambda_{13} + \lambda_{31}\lambda_{00} + \lambda_{30}\lambda_{01} + \lambda_{22}\lambda_{13} + \lambda_{23}\lambda_{12} - 2(\lambda_{33}\lambda_{01} + \lambda_{33}\lambda_{02} + \lambda_{33}\lambda_{10} + \lambda_{33}\lambda_{13} + \lambda_{33}\lambda_{20} + \lambda_{33}\lambda_{23} + \lambda_{33}\lambda_{31} + \lambda_{33}\lambda_{32} + 3\lambda_{33}\lambda_{33})\}]. \quad (\text{B16})$$

Appendix C: RG equations of source terms

After collecting all the one-loop corrections to source terms and performing RG analysis^{48,51,53}, we can obtain RG flow equations of the strengths $\Delta_i^{c/s}$ and Δ_i^{PP} corresponding to fermion-source terms in particle-hole and particle-particle situations,

$$\frac{d\Delta_1^c}{dl} = 2\Delta_1^c, \quad (\text{C1})$$

$$\begin{aligned} \frac{d\Delta_2^c}{dl} = & \left[2 + (\lambda_{00} - 7\lambda_{01} - \lambda_{02} - \lambda_{03} + \lambda_{10} + \lambda_{11} - \lambda_{12} - \lambda_{13} + \lambda_{20} + \lambda_{21} - \lambda_{22} - \lambda_{23} + \lambda_{30} + \lambda_{31} \right. \\ & \left. - \lambda_{32} - \lambda_{33}) \frac{(2d_3^2 + d_1^2)}{16\pi(d_3^2 + d_1^2)^{\frac{3}{2}}} \right] \Delta_2^c, \end{aligned} \quad (\text{C2})$$

$$\begin{aligned} \frac{d\Delta_3^c}{dl} = & \left[2 + (\lambda_{00} - \lambda_{01} - 7\lambda_{02} - \lambda_{03} + \lambda_{10} - \lambda_{11} + \lambda_{12} - \lambda_{13} + \lambda_{20} - \lambda_{21} + \lambda_{22} - \lambda_{23} + \lambda_{30} - \lambda_{31} \right. \\ & \left. + \lambda_{32} - \lambda_{33}) \frac{(2d_3^2 + d_1^2)}{16\pi(d_3^2 + d_1^2)^{\frac{3}{2}}} \right] \Delta_3^c, \end{aligned} \quad (\text{C3})$$

$$\begin{aligned} \frac{d\Delta_4^c}{dl} = & \left[2 + (\lambda_{00} - \lambda_{01} - \lambda_{02} - 7\lambda_{03} + \lambda_{10} - \lambda_{11} - \lambda_{12} + \lambda_{13} + \lambda_{20} - \lambda_{21} - \lambda_{22} + \lambda_{23} + \lambda_{30} - \lambda_{31} \right. \\ & \left. - \lambda_{32} + \lambda_{33}) \frac{d_1^2}{8\pi(d_3^2 + d_1^2)^{\frac{3}{2}}} \right] \Delta_4^c, \end{aligned} \quad (\text{C4})$$

$$\frac{d\Delta_1^s}{dl} = 2\Delta_1^s, \quad (\text{C5})$$

$$\begin{aligned} \frac{d\Delta_{2-x}^s}{dl} = & \left[2 + (\lambda_{00} + \lambda_{01} - \lambda_{02} - \lambda_{03} + \lambda_{10} - 7\lambda_{11} - \lambda_{12} - \lambda_{13} - \lambda_{20} - \lambda_{21} + \lambda_{22} + \lambda_{23} - \lambda_{30} - \lambda_{31} \right. \\ & \left. + \lambda_{32} + \lambda_{33}) \frac{(2d_3^2 + d_1^2)}{16\pi(d_3^2 + d_1^2)^{\frac{3}{2}}} \right] \Delta_{2-x}^s, \end{aligned} \quad (\text{C6})$$

$$\begin{aligned} \frac{d\Delta_{2-y}^s}{dl} = & \left[2 + (\lambda_{00} + \lambda_{01} - \lambda_{02} - \lambda_{03} - \lambda_{10} - \lambda_{11} + \lambda_{12} + \lambda_{13} + \lambda_{20} - 7\lambda_{21} - \lambda_{22} - \lambda_{23} - \lambda_{30} - \lambda_{31} \right. \\ & \left. + \lambda_{32} + \lambda_{33}) \frac{(2d_3^2 + d_1^2)}{16\pi(d_3^2 + d_1^2)^{\frac{3}{2}}} \right] \Delta_{2-y}^s, \end{aligned} \quad (\text{C7})$$

$$\begin{aligned} \frac{d\Delta_{2-z}^s}{dl} = & \left[2 + (\lambda_{00} + \lambda_{01} - \lambda_{02} - \lambda_{03} - \lambda_{10} - \lambda_{11} + \lambda_{12} + \lambda_{13} - \lambda_{20} - \lambda_{21} + \lambda_{22} + \lambda_{23} + \lambda_{30} - 7\lambda_{31} \right. \\ & \left. - \lambda_{32} - \lambda_{33}) \frac{(2d_3^2 + d_1^2)}{16\pi(d_3^2 + d_1^2)^{\frac{3}{2}}} \right] \Delta_{2-z}^s, \end{aligned} \quad (\text{C8})$$

$$\begin{aligned} \frac{d\Delta_{3-x}^s}{dl} = & \left[2 + (\lambda_{00} - \lambda_{01} + \lambda_{02} - \lambda_{03} + \lambda_{10} - \lambda_{11} - 7\lambda_{12} - \lambda_{13} - \lambda_{20} + \lambda_{21} - \lambda_{22} + \lambda_{23} - \lambda_{30} + \lambda_{31} \right. \\ & \left. - \lambda_{32} + \lambda_{33}) \frac{(2d_3^2 + d_1^2)}{16\pi(d_3^2 + d_1^2)^{\frac{3}{2}}} \right] \Delta_{3-x}^s, \end{aligned} \quad (\text{C9})$$

$$\begin{aligned} \frac{d\Delta_{3-y}^s}{dl} = & \left[2 + (\lambda_{00} - \lambda_{01} + \lambda_{02} - \lambda_{03} - \lambda_{10} + \lambda_{11} - \lambda_{12} + \lambda_{13} + \lambda_{20} - \lambda_{21} - 7\lambda_{22} - \lambda_{23} - \lambda_{30} + \lambda_{31} \right. \\ & \left. - \lambda_{32} + \lambda_{33}) \frac{(2d_3^2 + d_1^2)}{16\pi(d_3^2 + d_1^2)^{\frac{3}{2}}} \right] \Delta_{3-y}^s, \end{aligned} \quad (\text{C10})$$

$$\begin{aligned} \frac{d\Delta_{3-z}^s}{dl} = & \left[2 + (\lambda_{00} - \lambda_{01} + \lambda_{02} - \lambda_{03} - \lambda_{10} + \lambda_{11} - \lambda_{12} + \lambda_{13} - \lambda_{20} + \lambda_{21} - \lambda_{22} + \lambda_{23} + \lambda_{30} - \lambda_{31} \right. \\ & \left. - 7\lambda_{32} - \lambda_{33}) \frac{(2d_3^2 + d_1^2)}{16\pi(d_3^2 + d_1^2)^{\frac{3}{2}}} \right] \Delta_{3-z}^s, \end{aligned} \quad (\text{C11})$$

$$\frac{d\Delta_{4-x}^s}{dl} = \left[2 + (\lambda_{00} - \lambda_{01} - \lambda_{02} + \lambda_{03} + \lambda_{10} - \lambda_{11} - \lambda_{12} - 7\lambda_{13} - \lambda_{20} + \lambda_{21} + \lambda_{22} - \lambda_{23} - \lambda_{30} + \lambda_{31} \right.$$

$$+\lambda_{32}-\lambda_{33})\frac{d_1^2}{8\pi(d_3^2+d_1^2)^{\frac{3}{2}}}\Big]\Delta_{4-x}^s, \quad (\text{C12})$$

$$\begin{aligned} \frac{d\Delta_{4-y}^s}{dl} = & \left[2 + (\lambda_{00} - \lambda_{01} - \lambda_{02} + \lambda_{03} - \lambda_{10} + \lambda_{11} + \lambda_{12} - \lambda_{13} + \lambda_{20} - \lambda_{21} - \lambda_{22} - 7\lambda_{23} - \lambda_{30} + \lambda_{31} \right. \\ & \left. + \lambda_{32} - \lambda_{33})\frac{d_1^2}{8\pi(d_3^2+d_1^2)^{\frac{3}{2}}}\right]\Delta_{4-y}^s, \end{aligned} \quad (\text{C13})$$

$$\begin{aligned} \frac{d\Delta_{4-z}^s}{dl} = & \left[2 + (\lambda_{00} - \lambda_{01} - \lambda_{02} + \lambda_{03} - \lambda_{10} + \lambda_{11} + \lambda_{12} - \lambda_{13} - \lambda_{20} + \lambda_{21} + \lambda_{22} - \lambda_{23} + \lambda_{30} - \lambda_{31} \right. \\ & \left. - \lambda_{32} - 7\lambda_{33})\frac{d_1^2}{8\pi(d_3^2+d_1^2)^{\frac{3}{2}}}\right]\Delta_{4-z}^s, \end{aligned} \quad (\text{C14})$$

and

$$\begin{aligned} \frac{d\Delta_1^{\text{PP}}}{dl} = & \left\{ 2 + \left[\lambda_{01} + \lambda_{10} + \lambda_{12} + \lambda_{13} + \lambda_{20} + \lambda_{22} + \lambda_{23} + \lambda_{30} + \lambda_{32} + \lambda_{33} - (\lambda_{00} + \lambda_{02} + \lambda_{03} + \lambda_{11} \right. \right. \\ & \left. \left. + \lambda_{21} + \lambda_{31}) \right] \frac{d_3^2}{8\pi(d_3^2+d_1^2)^{\frac{3}{2}}} \right\} \Delta_1^{\text{PP}}, \end{aligned} \quad (\text{C15})$$

$$\begin{aligned} \frac{d\Delta_2^{\text{PP}}}{dl} = & \left\{ 2 + \left[\lambda_{03} + \lambda_{10} + \lambda_{11} + \lambda_{12} + \lambda_{20} + \lambda_{21} + \lambda_{22} + \lambda_{30} + \lambda_{31} + \lambda_{32} - (\lambda_{00} + \lambda_{01} + \lambda_{02} + \lambda_{13} \right. \right. \\ & \left. \left. + \lambda_{23} + \lambda_{33}) \right] \frac{d_1^2}{16\pi(d_3^2+d_1^2)^{\frac{3}{2}}} \right\} \Delta_2^{\text{PP}}, \end{aligned} \quad (\text{C16})$$

$$\begin{aligned} \frac{d\Delta_3^{\text{PP}}}{dl} = & \left\{ 2 + \left[\lambda_{02} + \lambda_{10} + \lambda_{11} + \lambda_{13} + \lambda_{20} + \lambda_{21} + \lambda_{23} + \lambda_{30} + \lambda_{31} + \lambda_{33} - (\lambda_{00} + \lambda_{01} + \lambda_{03} + \lambda_{12} \right. \right. \\ & \left. \left. + \lambda_{22} + \lambda_{32}) \right] \frac{1}{8\pi(d_3^2+d_1^2)^{\frac{1}{2}}} \right\} \Delta_3^{\text{PP}}, \end{aligned} \quad (\text{C17})$$

$$\begin{aligned} \frac{d\Delta_{4-x}^{\text{PP}}}{dl} = & \left\{ 2 + \left[\lambda_{01} + \lambda_{02} + \lambda_{03} + \lambda_{11} + \lambda_{12} + \lambda_{13} + \lambda_{20} + \lambda_{31} + \lambda_{32} + \lambda_{33} - (\lambda_{00} + \lambda_{10} + \lambda_{21} + \lambda_{22} \right. \right. \\ & \left. \left. + \lambda_{23} + \lambda_{30}) \right] \frac{d_1^2}{16\pi(d_3^2+d_1^2)^{\frac{3}{2}}} \right\} \Delta_{4-x}^{\text{PP}}, \end{aligned} \quad (\text{C18})$$

$$\begin{aligned} \frac{d\Delta_{4-y}^{\text{PP}}}{dl} = & \left\{ 2 + \left[\lambda_{01} + \lambda_{02} + \lambda_{03} + \lambda_{11} + \lambda_{12} + \lambda_{13} + \lambda_{21} + \lambda_{22} + \lambda_{23} + \lambda_{30} - (\lambda_{00} + \lambda_{10} + \lambda_{20} + \lambda_{31} \right. \right. \\ & \left. \left. + \lambda_{32} + \lambda_{33}) \right] \frac{d_1^2}{16\pi(d_3^2+d_1^2)^{\frac{3}{2}}} \right\} \Delta_{4-y}^{\text{PP}}, \end{aligned} \quad (\text{C19})$$

$$\begin{aligned} \frac{d\Delta_{4-z}^{\text{PP}}}{dl} = & \left\{ 2 + \left[\lambda_{01} + \lambda_{02} + \lambda_{03} + \lambda_{10} + \lambda_{21} + \lambda_{22} + \lambda_{23} + \lambda_{31} + \lambda_{32} + \lambda_{33} - (\lambda_{00} + \lambda_{11} + \lambda_{12} + \lambda_{13} \right. \right. \\ & \left. \left. + \lambda_{20} + \lambda_{30}) \right] \frac{d_1^2}{16\pi(d_3^2+d_1^2)^{\frac{3}{2}}} \right\} \Delta_{4-z}^{\text{PP}}, \end{aligned} \quad (\text{C20})$$

where the right hand sides of these equations are designated as $\mathcal{G}_i^{c/s,\text{PP}} \Delta_i^{c/s,\text{PP}}$ in Eq. (13).

* Corresponding author: jing-wang@tju.edu.cn

¹ K. S. Novoselov, A. K. Geim, S. V. Morozov, D. Jiang, M. I. Katsnelson, I. V. Grigorieva, S. V. Dubonos, and A. A. Firsov, *Nature* **438**, 197 (2005).

² A. H. Castro Neto, F. Guinea, N. M. R. Peres, K. S. Novoselov, and A. K. Geim, *Rev. Mod. Phys.* **81**, 109 (2009).

³ L. Fu, C. L. Kane, and E. J. Mele, *Phys. Rev. Lett.* **98**, 106803 (2007).

⁴ R. Roy, *Phys. Rev. B* **79**, 195322 (2009).

⁵ J. E. Moore, *Nature* **464**, 194 (2010).

⁶ M. Z. Hasan and C. L. Kane, *Rev. Mod. Phys.* **82**, 3045 (2010).

⁷ X. L. Qi and S. C. Zhang, *Rev. Mod. Phys.* **83**, 1057 (2011).

⁸ S. Q. Sheng, *Dirac Equation in Condensed Matter* (Berlin: Springer, 2012).

⁹ B. A. Bernevig and T. L. Hughes, *Topological Insulators and Topological Superconductors* (Princeton, NJ: Princeton University Press, 2013).

¹⁰ N. P. Armitage, E. J. Mele, and Ashvin Vishwanath, *Rev. Mod. Phys.* **90**, 015001 (2018).

- ¹¹ B. Roy and M. S. Foster, Phys. Rev. X **8**, 011049 (2018).
- ¹² H. K. Tang, J. N. Leaw, J. N. B. Rodrigues, I. F. Herbut, P. Sengupta, F. F. Assaad, and S. Adam, Science **361**, 570 (2018).
- ¹³ M. M. Korshunov, D. V. Efremov, A. A. Golubov, and O. V. Dolgov, Phys. Rev. B **90**, 134517 (2014).
- ¹⁴ H. H. Hung, A. Barr, E. Prodan, and G. A. Fiete, Phys. Rev. B **94**, 235132 (2016).
- ¹⁵ R. Nandkishore, J. Maciejko, D. A. Huse, and S. L. Sondhi, Phys. Rev. B **87**, 174511 (2013).
- ¹⁶ I. D. Potirniche, J. Maciejko, R. Nandkishore, and S. L. Sondhi, Phys. Rev. B **90**, 094516 (2014).
- ¹⁷ B. Roy and S. Das Sarma, Phys. Rev. B **94**, 115137 (2016).
- ¹⁸ R. M. Nandkishore and S. A. Parameswaran, Phys. Rev. B **95**, 205106 (2017).
- ¹⁹ B. Roy, Y. Alavirad, and J. D. Sau, Phys. Rev. Lett. **118**, 227002 (2017).
- ²⁰ B. Roy, R. J. Slager, and V. Juričić, Phys. Rev. X **8**, 031076 (2018).
- ²¹ B. Roy, V. Juričić, and S. D. Sarma, Sci. Rep. **6**, 32446 (2016).
- ²² Z. J. Wang, Y. Sun, X. Q. Chen, C. Franchini, G. Xu, H. M. Weng, X. Dai, and Z. Fang, Phys. Rev. B **85**, 195320 (2012).
- ²³ S. M. Young, S. Zaheer, J. C. Y. Teo, C. L. Kane, E. J. Mele, and A. M. Rappe, Phys. Rev. Lett. **108**, 140405 (2012).
- ²⁴ J. A. Steinberg, S. M. Young, S. Zaheer, C. L. Kane, E. J. Mele, and A. M. Rappe, Phys. Rev. Lett. **112**, 036403 (2014).
- ²⁵ Z. K. Liu, J. Jiang, B. Zhou, Z. J. Wang, Y. Zhang, H. M. Weng, D. Prabhakaran, S. K. Mo, H. Peng, P. Dudin, T. Kim, M. Hoesch, Z. Fang, X. Dai, Z. X. Shen, D. L. Feng, Z. Hussain, and Y. L. Chen, Nat. Mater. **13**, 677 (2014).
- ²⁶ Z. K. Liu, B. Zhou, Y. Zhang, Z. J. Wang, H. M. Weng, D. Prabhakaran, S. K. Mo, Z. X. Shen, Z. Fang, X. Dai, Z. Hussain, and Y. L. Chen, Science **343**, 864 (2014).
- ²⁷ J. Xiong, S. K. Kushwaha, T. Liang, J. W. Krizan, M. Hirschberger, W. Wang, R. J. Cava, and N. P. Ong, Science **350**, 413 (2015).
- ²⁸ A. A. Burkov and L. Balents, Phys. Rev. Lett. **107**, 127205 (2011).
- ²⁹ K. Y. Yang, Y. M. Lu, and Y. Ran, Phys. Rev. B **84**, 075129 (2011).
- ³⁰ X. G. Wan, A. M. Turner, A. Vishwanath, and S. Y. Savrasov, Phys. Rev. B **83**, 205101 (2011).
- ³¹ X. C. Huang, L. X. Zhao, Y. J. Long, P. P. Wang, D. Chen, Z. H. Yang, H. Liang, M. Q. Xue, H. M. Weng, Z. Fang, X. Dai, and G. F. Chen, Phys. Rev. X **5**, 031023 (2015).
- ³² S. Y. Xu, I. Belopolski, N. Alidoust, M. Neupane, G. Bian, C. L. Zhang, R. Sankar, G. Q. Chang, Z. J. Yuan, C. C. Lee, S. M. Huang, H. Zheng, J. Ma, D. S. Sanchez, B. K. Wang, A. Bansil, F. C. Chou, P. P. Shibayev, H. Lin, S. Jia, and M. Z. Hasan, Science **349**, 613 (2015).
- ³³ S. Y. Xu, N. Alidoust, I. Belopolski, Z. J. Yuan, G. Bian, T. R. Chang, H. Zheng, V. N. Strocov, D. S. Sanchez, G. Q. Chang, C. L. Zhang, D. X. Mou, Y. Wu, L. Huang, C. C. Lee, S. M. Huang, B. K. Wang, A. Bansil, H. T. Jeng, T. Neupert, A. Kaminski, H. Lin, S. Jia, and M. Z. Hasan, Nat. Phys. **11**, 748 (2015).
- ³⁴ B. Q. Lv, N. Xu, H. M. Weng, J. Z. Ma, P. Richard, X. C. Huang, L. X. Zhao, G. F. Chen, C. E. Matt, F. Bisti, V. N. Strocov, J. Mesot, Z. Fang, X. Dai, T. Qian, M. Shi, and H. Ding, Nat. Phys. **11**, 724 (2015).
- ³⁵ H. Weng, C. Fang, Z. Fang, B. A. Bernevig, and X. Dai, Phys. Rev. X **5**, 011029 (2015).
- ³⁶ Y. Hasegawa, R. Konno, H. Nakano, and M. Kohmoto, Phys. Rev. B **74**, 033413 (2006).
- ³⁷ S. Katayama, A. Kobayashi, and Y. Suzumura, J. Phys. Soc. Japan **75**, 054705 (2006).
- ³⁸ P. Dietl, F. Piechon, and G. Montambaux, Phys. Rev. Lett. **100**, 236405 (2008).
- ³⁹ V. Pardo and W. E. Pickett, Phys. Rev. Lett. **102**, 166803 (2009).
- ⁴⁰ P. Delplace and G. Montambaux, Phys. Rev. B **82**, 035438 (2010).
- ⁴¹ Y. Wu, Opt. Express **22**, 1906 (2014).
- ⁴² Y. D. Chong, X. G. Wen, and M. Soljačić, Phys. Rev. B **77**, 235125 (2008).
- ⁴³ K. Sun and E. Fradkin, Phys. Rev. B **78**, 245122 (2008).
- ⁴⁴ K. Sun, H. Yao, E. Fradkin, and S. A. Kivelson, Phys. Rev. Lett. **103**, 046811 (2009).
- ⁴⁵ O. Vafek, Phys. Rev. B **82**, 205106 (2010).
- ⁴⁶ O. Vafek and K. Yang, Phys. Rev. B **81**, 041401(R) (2010).
- ⁴⁷ V. Cvetković, R. E. Throckmorton, and O. Vafek, Phys. Rev. B **86**, 075467 (2012).
- ⁴⁸ J. M. Murray and O. Vafek, Phys. Rev. B **89**, 201110(R) (2014).
- ⁴⁹ I. F. Herbut, Phys. Rev. B **85**, 085304 (2012).
- ⁵⁰ W. Zhu, S. S. Gong, T. S. Zeng, L. Fu, and D. N. Sheng, Phys. Rev. Lett. **117**, 096402 (2016).
- ⁵¹ J. Wang, C. Ortix, J. van den Brink, and D. V. Efremov, Phys. Rev. B **96**, 201104(R) (2017).
- ⁵² Y. M. Dong, Y. H. Zhai, D. X. Zheng, and J. Wang, Phys. Rev. B **102**, 134204 (2020).
- ⁵³ B. Roy, arxiv: 2004.13043 (2020).
- ⁵⁴ I. Mandal and S. Gemsheim, Condens. Matter Phys. **22**, 13701 (2019).
- ⁵⁵ S. Ray, M. Vojta, and L. Janssen, Phys. Rev. B **102**, 081112(R) (2020).
- ⁵⁶ J. Shah and S. Mukerjee, arxiv: 2011.00249 (2020).
- ⁵⁷ I. Mandal and R. M. Nandkishore, Phys. Rev. B **97**, 125121 (2018).
- ⁵⁸ Y. P. Lin and R. M. Nandkishore, Phys. Rev. B **97**, 134521 (2018).
- ⁵⁹ J. M. Luttinger, Phys. Rev. **102**, 1030 (1956).
- ⁶⁰ S. Murakami, N. Nagaosa, and S. C. Zhang, Phys. Rev. B **69**, 235206 (2004).
- ⁶¹ L. Janssen and I. F. Herbut, Phys. Rev. B **92**, 045117 (2015).
- ⁶² I. Boettcher and I. F. Herbut, Phys. Rev. B **93**, 205138 (2016).
- ⁶³ L. Janssen and I. F. Herbut, Phys. Rev. B **95**, 075101 (2017).
- ⁶⁴ I. Boettcher and I. F. Herbut, Phys. Rev. B **95**, 075149 (2017).
- ⁶⁵ L. Savary, E. G. Moon, and L. Balents, Phys. Rev. X **4**, 041027 (2014).
- ⁶⁶ L. Savary, J. Ruhman, J. W. F. Venderbos, L. Fu, and P. A. Lee, Phys. Rev. B **96**, 214514 (2017).
- ⁶⁷ H. H. Lai, B. Roy, and P. Goswami, arXiv: 1409.8675 (2014).
- ⁶⁸ P. Goswami, B. Roy, and S. Das Sarma, Phys. Rev. B **95**, 085120 (2017).
- ⁶⁹ A. L. Szabo, R. Moessner, and B. Roy,

- arXiv:1811.12415 (2018).
- ⁷⁰ B. Roy, Sayed Ali Akbar Ghorashi, M. S. Foster, and A. H. Nevidomskyy, Phys. Rev. B **99**, 054505 (2019).
 - ⁷¹ S. Ray, M. Vojta, and L. Janssen, Phys. Rev. B **98**, 245128 (2018).
 - ⁷² J. R. Wang, W. Li, and C. J. Zhang, Phys. Rev. B **102**, 085132 (2020).
 - ⁷³ G. W. Chern and C. D. Batista, Phys. Rev. Lett. **109**, 156801 (2012).
 - ⁷⁴ W. F. Tsai, C. Fang, H. Yao, and J. Hu, New J. Phys. **17**, 055016 (2015).
 - ⁷⁵ Y. Xiao, V. Pelletier, P. M. Chaikin, and D. A. Huse, Phys. Rev. B **67**, 104505 (2003).
 - ⁷⁶ J. W. F. Venderbos, M. Manzardo, D. V. Efremov, J. van den Brink, and C. Ortix, Phys. Rev. B **93**, 045428 (2016).
 - ⁷⁷ H. Q. Wu, Y. Y. He, C. Fang, Z. Y. Meng, and Z. Y. Lu, Phys. Rev. Lett. **117**, 066403 (2016).
 - ⁷⁸ R. Shankar, Rev. Mod. Phys. **66**, 129 (1994).
 - ⁷⁹ K. G. Wilson, Rev. Mod. Phys. **47**, 773 (1975).
 - ⁸⁰ J. Polchinski, arXiv: hep-th/9210046 (1992).
 - ⁸¹ S. Maiti and A. V. Chubukov, Phys. Rev. B **82**, 214515 (2010).
 - ⁸² A. Altland and B. Simons, *Condensed Matter Field Theory* (Cambridge University Press, Cambridge, 2006).
 - ⁸³ M. Vojta, Rep. Prog. Phys. **66**, 2069 (2003).
 - ⁸⁴ C. J. Halboth and W. Metzner, Phys. Rev. Lett. **85**, 5162 (2000).
 - ⁸⁵ C. J. Halboth and W. Metzner, Phys. Rev. B **61**, 7364 (2000).
 - ⁸⁶ J. Wang, A. Eberlein, and W. Metzner, Phys. Rev. B **89**, 121116(R) (2014).
 - ⁸⁷ A. V. Chubukov, Annu. Rev. Condens. Matter Phys. **3**, 57 (2012).
 - ⁸⁸ A. V. Chubukov, M. Khodas, and R. M. Fernandes, Phys. Rev. X **6**, 041045 (2016).
 - ⁸⁹ J. Wang and G. Z. Liu, Phys. Rev. D **85**, 105010 (2012).
 - ⁹⁰ A. Altland, B. D. Simons, and M. R. Zirnbauer, Phys. Rep. **359**, 283 (2002).
 - ⁹¹ A. W. W. Ludwig, M. P. A. Fisher, R. Shankar, and G. Grinstein, Phys. Rev. B **50**, 7526 (1994).
 - ⁹² C. Xu, Y. Qi, and S. Sachdev, Phys. Rev. B **78**, 134507 (2008).
 - ⁹³ J. R. Wang, G. Z. Liu, and C. J. Zhang, New J. Phys. **18**, 073023 (2016).
 - ⁹⁴ J. Wang, P. L. Zhao, J. R. Wang, and G. Z. Liu, Phys. Rev. B **95**, 054507 (2017).
 - ⁹⁵ Y. M. Dong, D. X. Zheng, and J. Wang, J. Phys.: Condens. Matter **31**, 275601 (2019).
 - ⁹⁶ J. Wang, J. Phys: Condens. Matter **30**, 125401 (2018).
 - ⁹⁷ J. Wang, G. Z. Liu, and H. Kleinert, Phys. Rev. B **83**, 214503 (2011).
 - ⁹⁸ Y. Huh and S. Sachdev, Phys. Rev. B **78**, 064512 (2008).
 - ⁹⁹ J. Wang, Phys. Rev. B **87**, 054511 (2013).
 - ¹⁰⁰ J. H. She, J. Zaanen, A. R. Bishop, and A. V. Balatsky, Phys. Rev. B **82**, 165128 (2010).
 - ¹⁰¹ E. A. Kim, M. J. Lawler, P. Oreto, S. Sachdev, E. Fradkin, and S. A. Kivelson, Phys. Rev. B **77**, 184514 (2008).
 - ¹⁰² J. H. She, M. J. Lawler, and E. A. Kim, Phys. Rev. B **92**, 035112 (2015).
 - ¹⁰³ B. Roy, P. Goswami, and J. D. Sau, Phys. Rev. B **94**, 041101(R) (2016).
 - ¹⁰⁴ T. Stauber, F. Guinea, and M. A. H. Vozmediano, Phys. Rev. B **71**, 041406(R) (2005).
 - ¹⁰⁵ R. Nandkishore, L. S. Levitov, and A. V. Chubukov, Nat. Phys. **8**, 158 (2012).
 - ¹⁰⁶ A. L. Szabó and B. Roy, arXiv: 2009.05055 (2020).
 - ¹⁰⁷ J. Wang, *Topological superconducting transition driven by time-reversal-symmetry breaking*, Nuclear Physics B, <https://doi.org/10.1016/j.nuclphysb.2020.115230> (2020).
 - ¹⁰⁸ Y. P. Lin and R. M. Nandkishore, arXiv: 2008.05485 (2020).
 - ¹⁰⁹ V. Saran, M. Karmakar, and R. Ganesh, Phys. Rev. B **100**, 104520 (2019).
 - ¹¹⁰ Y. Tada, Phys. Rev. Research **2**, 033363 (2020).
 - ¹¹¹ M. J. Trott and C. A. Hooley, arXiv: 2004.06665 (2020).
 - ¹¹² D. Sehayek, M. Thakurathi, and A. A. Burkov, Phys. Rev. B **102**, 115159 (2020).
 - ¹¹³ P. A. Lee, N. Nagaosa, and X. G. Wen, Rev. Mod. Phys. **78**, 17 (2006).
 - ¹¹⁴ E. Fradkin, S. A. Kivelson, M. J. Lawler, J. P. Eisenstein, and A. P. Mackenzie, Annu. Rev. Condens. Matter Phys. **1**, 153 (2010).
 - ¹¹⁵ S. Das Sarma, S. Adam, E. H. Hwang, and E. Rossi, Rev. Mod. Phys. **83**, 407 (2011).
 - ¹¹⁶ S. Sachdev, *Quantum Phase Transitions 2nd edn* (Cambridge: Cambridge University Press, 2011).
 - ¹¹⁷ V. N. Kotov, B. Uchoa, V. M. Pereira, F. Guinea, and A. H. Castro Neto, Rev. Mod. Phys. **84**, 1067 (2012).
 - ¹¹⁸ G. Mahan, *Many-Particle Physics, 2nd edn.* (Plenum, New York, 1990).
 - ¹¹⁹ J. I. Kapusta and C. Gale, *Finite-Temperature Field Theory: Principles and Applications* (Cambridge, UK; New York, 1994).
 - ¹²⁰ I. S. Gradshteyn and I. M. Ryzhik, *Table of Integrals, Series, and Products, 7th edn.* (Academic Press, America, 2007).
 - ¹²¹ D. E. Sheehy and J. Schmalian, Phys. Rev. Lett. **99**, 226803 (2007).
 - ¹²² F. Schwabl, *Statistical Mechanics* (Springer, Berlin, 2006), 2nd ed., p. 85.
 - ¹²³ E. H. Hwang, Ben Yu-Kuang Hu, and S. Das Sarma, Phys. Rev. Lett. **99**, 226801 (2007).